

**Enhancing Gold Recovery from Nevada Double Refractory  
Gold Ores using a Novel Dual Bubble Generator**

by

Jian Huang

A thesis submitted in partial fulfillment of the requirements for the degree of

**Master of Science**

in

**Chemical Engineering**

Department of Chemical and Materials Engineering  
University of Alberta

© Jian Huang, 2018

## ABSTRACT

In this study, the influence of dual bubble generator on mineral flotation was investigated. A Venturi-based dual bubble generator was designed and characterized in both liquid-gas two-phase system and solid-liquid-gas three-phase flotation system. The dual bubble generator featured immediated contact of fresh micron size bubbles generated by hydrodynamic cavitation with conventional flotation size bubbles produced by forcing the air through ceramic sparger into the liquid downstream of the Venturi tube, reducing bubble aging and hence the bubble-particle induction time. In the two-phase system, the influence of the gas injection rate, gas injection point, fluid velocity and addition of frother on the size of bubbles and gas hold up was investigated. In the three-phases flotation test, the effect of different flotation methods and different bubble generators on fine particle flotation was studied. Increasing gas injection rate was found to increase both the gas hold up and bubble size. Increasing the frother concentration led to an increase in gas hold up but a decreased in the size of bubbles. Injection of gas at Venturi port (G1) generated small bubbles while injection of gas at expanding zone after Venturi (G2) led to generation of large bubbles. The use of the dual bubble generator was found to enhance both the fine gold recovery and the gold grade of the concentrate.

## ACKNOWLEDGMENTS

I would like to express my sincere gratitude to Professor Zhenghe Xu and Professor Qingxia (Chad) Liu, my supervisors for their enthusiastic encouragement and support during my graduate studies.

I would also like to extend my thanks to Mr. John Jiang and Mr. Mike Zhou from AuTec Innovative Extractive Solutions Ltd.. Without their help, I would not have been able to finish the onsite test.

I would like to thank Mr. Haipeng Li who gave me great hands on a good start of the project. My grateful thanks are also extended to Professor Gongzhen Li, Professor Ge Zhang, Professor Xitao Wang, Mr. Qiming Fan and Dr. Yang Fan, whose valuable suggestions greatly accelerated the project progress.

I would like to thank Mr. Carl Corbett, Mr. Jim Skwarok and Ms. Jie Ru who constantly provided me with valuable information and the instrument trainings. Special thanks should be given to Mr. Herb Green who helped me to build the bubble generator, flotation column system and bubble view analysis system.

I would like to thank Mr. Mingda Li and Mr. Vitalii Dodonov for their help on re-running some of the tests. My thanks also extend to my colleagues in Oil Sands Industrial Research Chair program for all their support and assistance.

I would like to acknowledge the financial support from Natural Science and Engineering Research Council of Canada (NSERC), the Canadian Centre for Clean Coal/Carbon and Mineral Processing Technologies (C<sup>5</sup>MPT) and Canadian Mining Industry Research Organization (CAMIRO).

Finally, I would like to thank my father (Mr. Liangjian Huang) and my mother (Ms. Yuhong Chen) for their encouragement.

# Table of Contents

<b>Chapter 1 Introduction</b> .....	1
1.1 Background .....	1
1.2 Objectives and organization of the thesis.....	4
<b>Chapter 2 Literature Review</b> .....	6
2.1 Different types of flotation devices.....	6
2.2 Different types of bubble generators.....	9
2.3 Fine particle flotation.....	12
2.4 Design concept of a dual bubble generator .....	16
2.5 Hydrodynamic cavitation .....	17
2.5.1 Mechanical agitation.....	17
2.5.2 Fast liquid flow.....	18
2.5.3 Dissolved gas content. ....	18
2.6 Bubble view analyses .....	19
<b>Chapter 3 Experimental Setup and Procedures</b> .....	20
3.1 Two-phase column flotation test setup.....	21
3.2 Two-phase column flotation test methods .....	27
3.3 Three-phase column flotation setup.....	28
3.4 Three-phase column flotation test procedures .....	30
<b>Chapter 4 Experimental Results and Discussion</b> .....	33

4.1	Two-phase column flotation tests.....	33
4.1.1	Bubble size.....	33
4.1.2	Gas hold up .....	39
4.2	Three -phase column flotation tests .....	48
4.2.1	G1, G2 injection rate.....	48
4.2.2	Froth depth .....	49
4.2.3	Cavitation pump circulating rate .....	50
4.2.4	Comparison of long and short column using the dual bubble generator ...	51
4.2.5	Comparison of the commercial bubble generator, dual bubble generator and Denver cell.....	52
<b>Chapter 5 Summary and Conclusions .....</b>		<b>59</b>
<b>Chapter 6 Future Work and Recommendations .....</b>		<b>60</b>
<b>References .....</b>		<b>61</b>
<b>Appendix.....</b>		<b>67</b>

## List of Figures

Figure 1-1. Typical relationships between flotation recovery and particle size.....	2
Figure 1-2 Effect of bubble aging on coalescence time of bubbles .....	3
Figure 2-1 Schematics of a mechanical cell .....	7
Figure 2-2 Schematics of flotation column.....	8
Figure 2-3 Schematics of a reactor/seperator cell.....	9
Figure 2-4 Design parameters of a venturi-type bubble generator (Unit: mm) ...	11
Figure 2-5 Evolution of bubble breakup at different injection ports diameters ( $d_i=1$ mm (a), $d_i=1.5$ mm (b), $d_i=2$ mm (c), $d_i=2.5$ mm (d), $d_i=3$ mm (e). ....	11
Figure 2-6 Geometry of the vortex generator and three configurations of the pipe .....	12
Figure 2-7 Schematics of a cyclonic-static micro-bubble flotation column (FCSMC) .....	12
Figure 2-8 Schematic diagram of a two-stage aeration system .....	15
Figure 2-9 Schematics of a hydrodynamic cavitation-based commercial bubble generator (a) and novel dual bubble generator (b).....	16
Figure 3-1 Schematics of flotation column used for the two-phase tests .....	20
Figure 3-2 Schematics of flotation column used for the three-phase flotation tests of gold ores .....	21
Figure 3-3 Schematics of a McGill bubble size analyzer.....	22
Figure 3-4 Calibration chart of pumps.....	24
Figure 3-5 Measurement of gas holdup by pressure difference: (a) general and (b) using water monometer.....	27

Figure 3-6 Original image of bubble (Top left), the image transformed to grey scales (Top right), image made into binary by a thresholding value while keeping the edges (Bottom left), find the circles (Bottom right), and count the number and calculate the average diameter of bubbles .....	27
Figure 3-7 Flotation concentrate (Left) and, tailings (Right) of BR20.....	32
Figure 4-1 Bubble size distribution of air injected only from G1.....	34
Figure 4-2 Bubble size distribution of air injected only from G2.....	34
Figure 4-3 Bubble size distribution of air injected only from G1 and G2 .....	35
Figure 4-4 Effect of G2 on bubble size.....	36
Figure 4-5 Effect of G2 on bubble size.....	36
Figure 4-6 Effect of G1 and G2 on bubble size .....	36
Figure 4-7 Effect of gas injection rate on bubble size .....	38
Figure 4-8 Effect of MIBC concentration on bubble size.....	39
Figure 4-9 Gas holdup as a function of airflow rate, which injected at G1 and G2, respectively.....	41
Figure 4-10 Gas holdup as a function of airflow rate injected at G1 or G2, with 10 ppm MIBC added.....	43
Figure 4-11 Gas holdup as a function of airflow rate, injected at G1 or G2, with 20 ppm MIBC added.....	43
Figure 4-12 Effect of MIBC concentration on gas holdup .....	44
Figure 4-13 Effect of gas flow rate in G1 on overall gas holdup.....	46

Figure 4-14 Effect of gas flow rate in G2 on overall gas holdup.....	46
Figure 4-15 Air flow rate at G2 vs mass pull and gold recovery.....	48
Figure 4-16 Air flow rate at G1 vs mass pull and gold recovery.....	49
Figure 4-17 Froth depth vs mass pull and recovery.....	50
Figure 4-18 Circulating flow rate vs. mass pull and gold recovery.....	50
Figure 4-19 Gold recovery vs mass pull for short and long column .....	51
Figure 4-20 Sulfide recovery vs mass pull for short and long column.....	52
Figure 4-21 TCM recovery vs mass pull for short and long column.....	52
Figure 4-22 Au, TCM, S Recovery from flotation column with commercial bubble generator, dual bubble generator and Denver cell of rougher and scavenger flotation.....	53
Figure 4-23 Effect of mass pull on gold recovery using Denver flotation cell and flotation column with commercial bubble generator .....	55
Figure 4-24 Gold grade-recovery curve obtained using Denver flotation cell and flotation column with commercial bubble generator .....	55
Figure 4-25 Effect of mass pull on gold recovery in flotation column with dual bubble generator or commercial bubble generator .....	57
Figure 4-26 Gold grade-recovery curve obtained using flotation column with dual bubble generator or commercial bubble generator .....	57

## **List of Tables**

Table 3-1 BR20 head assay .....	29
Table 3-2 BR20 ore mineralogy .....	29
Table 4-1 Flotation results from commercial bubble generator, dual bubble generator and Denver cell	53

## NOMENCLATURE

$P_c$	probability of bubble–particle collision
$P_a$	probability of bubble/particle attachment
$P_d$	probability of bubble/particle detachment
R	fine particle recovery
$D_p$	diameters of particles
$D_b$	diameters of bubbles
$P_A$	pressure at location A
$P_B$	pressure at location B
$\rho_{sl}$	density of slurry in column
g	gravitational acceleration
$L_A$	vertical distance between point A and water level
$L_B$	vertical distance between point B and water level
$\varepsilon_A$	volume fraction of air at point A
$\varepsilon_B$	volume fraction of air at point B
$\varepsilon_g$	volume fraction of air between points A and B in the column
$\Delta h$	vertical distance from manometer reading

# **Chapter 1 Introduction**

## **1.1 Background**

Flotation represents a unit operation in which solids are separated from one another depending on their differences in surface characteristics. It is also a selective process for separating minerals from gangue by using surfactants known as collectors. The selective separation of the minerals makes processing complex ores economically feasible. In froth flotation process, the hydrophobic mineral particles will attach to rising bubbles in a flotation device due to the hydrophobic driving force between the mineral particles and gas bubbles (Yoon et al.,1997). The gas bubbles and hydrophobic mineral particles then becomes the bubble/particle aggregates. If the density of bubble/particle aggregates is less than the density of the liquid phase, the bubble/particle aggregates will float to the top froth layer by buoyancy force. In the same time, the hydrophilic particles will not attach to the gas bubbles. This kind of particles will discharge from the bottom of the flotation cell or flotation column as tailings.

However, flotation has been proven inefficient for fine particles although it becomes increasingly inevitable to process fine particles with the depletion of easy processing ores. The relationship between flotation recovery and particle size is shown in Figure 1-1(Feng and Aldrich, 1999).

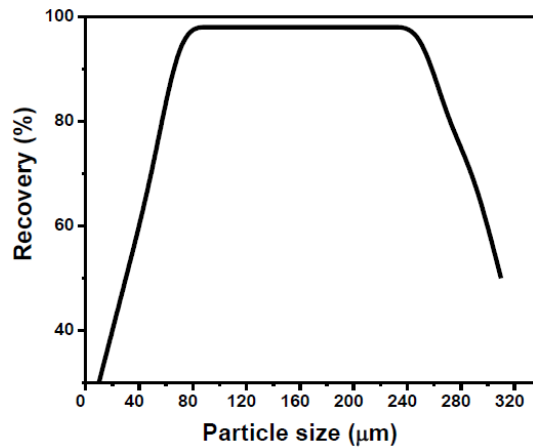


Figure 1-1. Typical relationship between flotation recovery and particle size

For conventional flotation, when the particle size is in the range of 50 μm to 250 μm, the good recovery can be obtained (Tao, 2004). The recovery of fine particles reduced drastically when the particle size is smaller than 50 μm.

To improve fine particle flotation, micron size bubbles were introduced to conventional flotation process. Sobhy and Tao (2013) and Zhou et al. (2009) pointed out that the micron size bubbles could lead to aggregation of hydrophobic fine particles, which increases the apparent particle size. The collision probability and attachment probability between gas bubbles and fine particles increase by increasing the particle size. The fine particle recovery could then be enhanced by adding micron size bubbles.

Many researchers have shown that micron size bubbles can be generated by many methods. The micron size bubbles generated by hydrodynamic cavitation method are widely used in fine particle flotation. The bubble size can be controlled by adjusting the pressure, liquid or slurry flow velocity, gas concentration and geometry of cavitation device (Moholkar and Pandit, 1997; Gogate and Pandit, 2005; Li et al., 2015).

However, the micron size bubble cannot provide sufficient buoyancy force to float mineral particles. Therefore, the flotation size bubbles are still required in the flotation process (Nesset et al., 2006). The coalescence time of aging bubbles is shown in Figure 1-2 (Li et al., 2015). The results show that the bubble aging is detrimental to bubble coalescence.

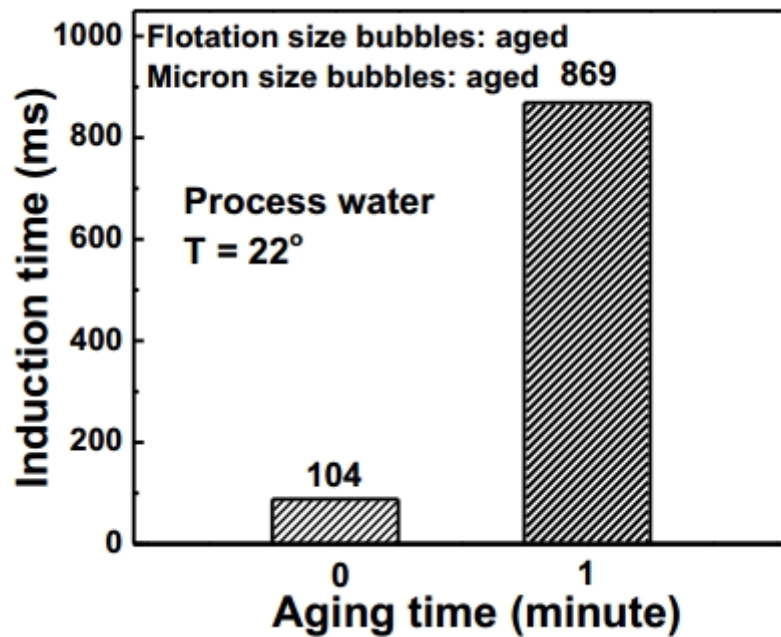


Figure 1-2 Effect of bubble aging on coalescence time of bubbles

There is another key issue of bubble/particle attachment that we need to be considered. In the flotation process, bubbles are generated in the pulp. Both micron size bubbles and flotation size bubbles are possible to be aged. Wang (2013) pointed out that bubble aging will affect the bubble/particle attachment.

A special sparger to produce both micron size bubbles and conventional flotation size bubbles has been developed by University of Alberta. It employs selective gas nucleation in situ on hydrophobic particles by hydrodynamic cavitation. The

aggregation of hydrophobic fine particles induced by gas nucleation has been observed to increase apparent particle sizes, thus making them more favorable for the attachment onto conventional flotation bubbles. This finding suggests that hydrodynamic cavitation on hydrophobic particles could improve the recovery and the selectivity of fine particle froth flotation with respect to hydrophilic gangue minerals. By testing a two-stage bubble attachment process, such as small gas bubbles nucleated on hydrophobic particles and then attachment onto conventional bubbles, much better flotation behavior than one stage bubble-particle attachment due to shorter induction time (thin film rupture time) and better flotation recovery were obtained. The column with dual bubble generator clearly yielded a consistently 6% higher recovery in gold compared to the column with commercial bubble generator operating with the same reagent scheme and mass pull.

## **1.2 Objectives and Organization of the thesis**

The present thesis describes the benefits of using a hydrodynamic cavitation-based dual bubble generator in column flotation to recover fine gold from a Nevada double refractory gold ore. The effect of fluid velocity, dissolved gas content, and addition of frother on the hydrodynamic cavitation in air/water (homogenous nucleation) system and the interaction between micron size bubbles and fine particles was investigated.

In Chapter 1, challenges of fine particle flotation are introduced. In Chapter 2, the types of flotation devices and bubble generators, key issues of fine particle flotation and bubble aging, design concept of bubble generators, hydrodynamic cavitation and

McGill bubble analyzer are reviewed. In Chapter 3, the experimental setup and procedures for investigation of bubble size, gas holdup and gold recovery are described. In Chapter 4, the experimental results are reported and discussed. In Chapter 5, the results obtained are summarized and in Chapter 6, future work regarding the hydrodynamic cavitation for fine particle flotation is proposed.

## Chapter 2 Literature Review

### 2.1 Different types of flotation devices

Froth flotation is a process for physically separating valuable minerals from the rocks (gangues) in aqueous slurry based on the differences in surface wettability of minerals.

According to Finch (1995), there are three main types of flotation devices: mechanical cells, flotation columns and reactor/separator cells.

The first type of the flotation device is the mechanical cells. Mechanical cells use a mechanical agitation method to cause flotation. The flotation process generally consists of several stages including roughing, scavenging and cleaning. In a mechanical flotation cell, the air and slurry fully mixed by impeller agitation. During this process, the air bubbles attach to the hydrophobic particles in the slurry and travel to the top of the cell. The rest of the slurry becomes tailings. In order to improve the grade of the products (concentrates), the mechanical flotation cell in some cases also uses wash water to create a downward stream to reduce the number of entrained particles in the froth back into the froth zone. The mechanical flotation cell has a good performance in large particle flotation but poor capability in fine particle flotation. A schematic of a mechanical flotation cells is shown in Figure 2-1

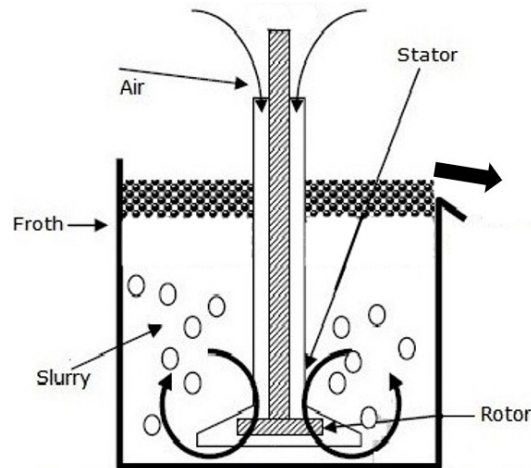


Figure 2-1 Schematics of a mechanical cell

The second type of flotation device is flotation column. The flotation column was invented in 1962, and the first commercial flotation column was introduced at Mines Gaspé. A 0.51-m square column was used for Molybdenum (Mo) cleaning (Coffin, 1982). In a conventional flotation column, feed enters just below the froth zone while the air bubbles rise in the column from a bubble generator near the bottom of the column. As the bubbles rise from the bottom of the column, air bubbles attach to the hydrophobic particles and gather on the top of the column. Wash water is often introduced at the top of the column to push the entrained fine particles back to the bubbly zone, while the washed froth overflows into the launder and is collected as the concentrate. The tailings are discharged from the bottom. Compared to the mechanical cell, the column flotation has many advantages such as improved mineral recovery, higher grade of the concentrate and lower operation costs. A schematic of a conventional flotation column is shown in Figure 2-2:

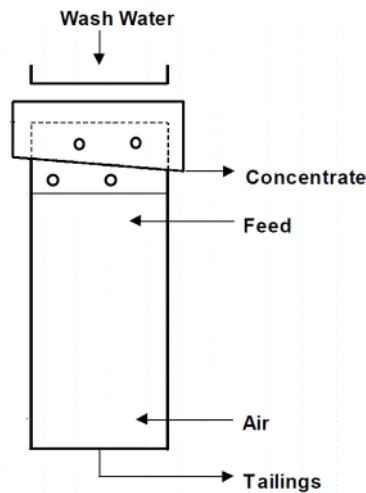


Figure 2-2 Schematics of flotation column

The third type of flotation devices is reactor/ separator cell. The main function of flotation cell is to attach hydrophobic particles to air bubbles, and to separate the aggregates from the cell. The main difference between the reactor/separator cell and mechanical flotation cell is that the reactor/separator cell can be separated into two parts, with the reactor part encouraging bubble and particle attachments (slurry was mixed with entrained air in an agitation box) and the separator part for separation and gathering the products. The reactor/separator cells can achieve better separation performances (higher particle collection rates, reduced cell height and higher capacity) in comparison with mechanical flotation cells. A schematic of a reactor/separator cell is shown in Figure 2-3

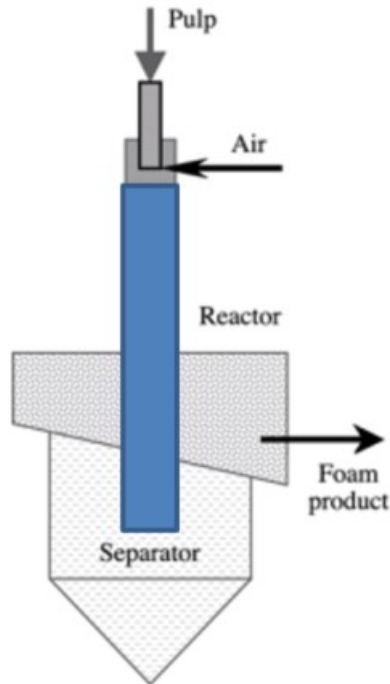


Figure 2-3 Schematics of a reactor/separator cell

## 2.2 Different types of bubble generators

Since the late 1970s, a number of fine bubble generation techniques have been developed based on hydrodynamic cavitation, ultrasonic oscillation and electrolysis (Li, et al., 2015). A feasible and simple bubble generator is the Venturi type bubble generator first developed by Kress (1972), which proved to be successful in breaking large bubbles into very small bubbles for the mineral industry. Hydrodynamic cavitation can greatly enhance mass transfer rate and features lower energy consumption and maintenance difficulty with easier installation than ultrasonic, and electrolysis methods. Venturi type bubble generator is easy to design and apply and lowers the bubble size and hence the particle size limit of effective flotation compared with the technologies that operate in traditional flotation units.

The bubble breakup mechanism of Venturi type bubble generator is due to the pressure shock induced by the transition from supersonic flow to subsonic flow, along with the turbulence from the liquid phase that splits the gas-liquid interphase (Li, et. al., 2017). Tao et al. (2008) and Sobhy and Tao (2013) confirmed that hydrodynamic cavitation of Venturi bubble generator could enhance fine phosphate particle flotation recovery. Canadian Process Technologies Inc. (CPT) already applied hydrodynamic cavitation in fine particle flotation and conducted pilot tests on the cavitation systems at several Brazilian phosphate flotation plants. The results from such pilot plant tests showed that installing a hydrodynamic cavitation sparger increased phosphate flotation recovery by 2–3% (Eriez, 2013).

Li, et. al. (2017) adopted a Venturi type bubble generator in the gas removal system for the liquid-fuel thorium molten salt reactor. The effect of three main geometrical parameters, including the injection port diameter, injection port number, and divergent angle, on bubble size distributions was clarified. According to the high-speed visualization and post processing algorithm, the injection hole diameter and the number of injection hole showed little effect on the bubble size distribution while the divergent angle is proved to be sensitive. The geometrical parameters and fine bubbles in Venturi type bubble generator are shown in Figures 2-4 and 2-5, respectively.

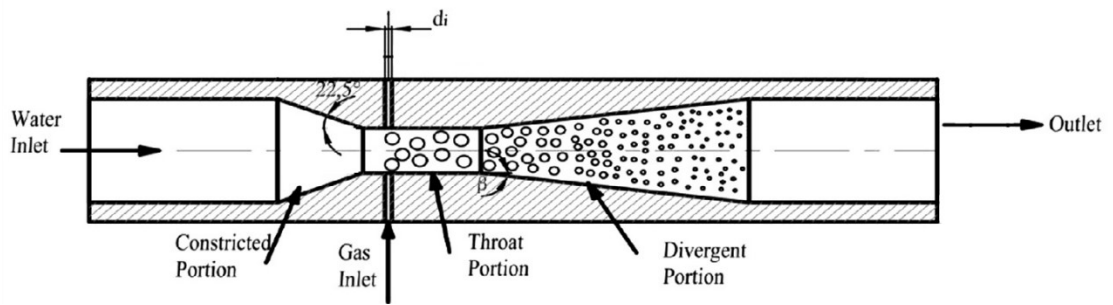


Figure 2-4 Design parameters of a venturi-type bubble generator (Unit: mm) (Li, et. al., 2017)

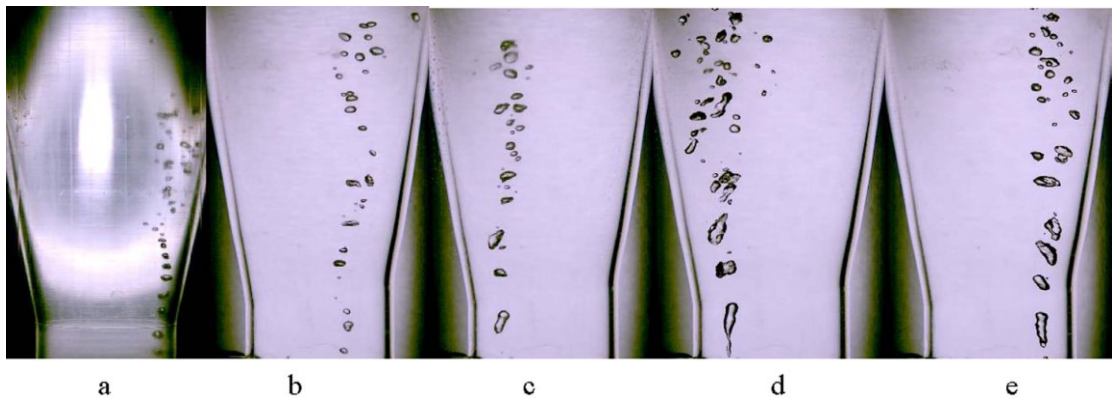


Figure 2-5 Evolution of bubble breakup at different injection ports diameters ( $d_i=1$  mm (a),  $d_i=1.5$  mm (b),  $d_i=2$  mm (c),  $d_i=2.5$  mm (d),  $d_i=3$  mm (e) (Li, et. al., 2017)

Vortex generator (VG) is another technique to generate fine bubbles. Wang et. al., (2017) investigated the recovery of fine-grained minerals with vortex generators in pipe flow unit of a cyclonic-static micro-bubble flotation column. Using numerical simulations, the optimal VG configurations of pipe flow and arrays arrangement in the pipe flow unit are obtained as shown in Figure 2-6. The schematics of a cyclonic-static micro-bubble flotation column (FCSMC) is shown in Figure 2-7. The modified FCSMC structures can enhance the yield and the combustible recovery of coal slime from a China coal preparation plant (Linhuan coal preparation plant), hence improving flotation performance. Yan et al. (2012) also reported that the recovery of fine-grained

mineral can be enhanced by increasing the turbulence level in the pipe flow unit in a FCSMC.

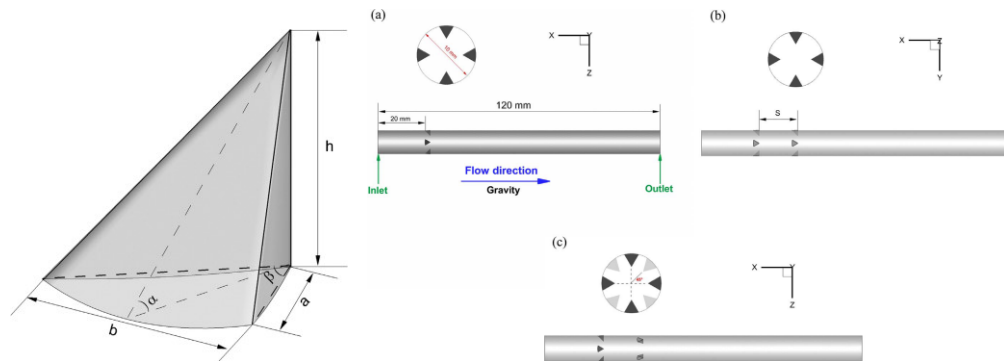


Figure 2-6 Geometry of the vortex generator and three configurations of the pipe flow unit (a) Single array, (b) Aligned dual arrays and (c) Staggered dual arrays. Wang (2017)

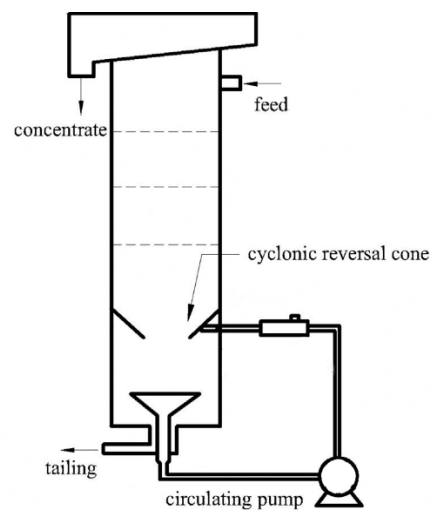


Figure 2-7 Schematic of a cyclonic-static micro-bubble flotation column (FCSMC) (Wang et al., 2015)

### 2.3 Fine particle flotation

The critical problem of fine particle flotation is the low attachment efficiency of fine particles to flotation size bubbles due to their low collision rate. In the flotation process, the fine particle recovery,  $R$  is determined by three micro-scale processes defined as:

$$R = F[P_c P_a (1 - P_d)] \quad (1)$$

where  $P_c$  is the probability of bubble–particle collision,  $P_a$  is the efficiency of bubble/particle attachment,  $P_d$  is the probability of bubble/particle detachment,  $F$  is a constant number,  $R$  is fine particle recovery. (Yoon and Luttrell, 1986; Tao 2005) The probability of collision,  $P_c$  can be quantified as the fraction of particles that collide with bubbles (Weber and Paddock 1983; Yoon and Luttrell, 1986) defined as

$$P_c = F(D_p/D_b) \quad (2)$$

where  $D_p$  and  $D_b$  are diameters of particles and bubbles, respectively. Bubble size and particle size impact the bubble-particle collision in opposite directions. It is evident that the probability of bubble–particle collision decreases with decreasing the size of particles, leading to a low recovery of fine particles. In this case, reducing the bubble size and/or increasing the apparent size of particles by fine particle aggregation are clear means to improve fine particle recovery.

Hydrodynamic cavitation generates micron size bubbles on the hydrophobic particle surfaces by in situ gas nucleation, which was found to be beneficial to fine particle flotation (Sobhy and Tao, 2013). In situ gas nucleation by hydrodynamic cavitation on hydrophobic surfaces occurs when the local pressure of the liquid drops below its vapor pressure. Hydrodynamic cavitation here is specifically referred to as the creation of gas nuclei through pressure reduction achieved by increasing the fluid velocity (Brennen, 1995; Hu et al., 1998). Gas nucleates favorably on rough and hydrophobic surfaces of solid particles, which increases the probability of bubble–particle collision (Zhou et al., 2009). The micron size bubbles generated by hydrodynamic cavitation could function

as a secondary collector, improving the probability of attachment between conventional flotation bubbles and fine particles frosted with cavitation bubbles (Zhou et al., 1997; Luttrell and Yoon, 1992). Laboratory tests confirmed that use of bubbles generated by hydrodynamic cavitation not only increased the coal flotation recovery, but also reduced the dosage of flotation reagents by using hydrodynamic cavitation bubble generator in column flotation systems (Tao et al., 2008; Sobhy and Tao, 2013). A recent pilot plant test using hydrodynamic cavitation bubble generator showed an increase in phosphate recovery by 2-3% (ERIEZ, 2015). However, the use of fine bubbles generated by hydrodynamic cavitation alone is not sufficient to achieve efficient particle recovery due to limited gas holdup that could be generated and low buoyancy of fine bubbles (Li, et al. 2015). It is therefore of great incentive to improve flotation recovery by introducing conventional flotation size bubbles in hydrodynamic cavitation based flotation systems.

The concept of two-stage aeration was present by Zhou et al. (2010) and Tao et al. (2006). The Schematic diagram of the two-stage aeration concept in flotation is shown in the Figure 2-8 (57th Canadian chemical engineering conference, 2007).

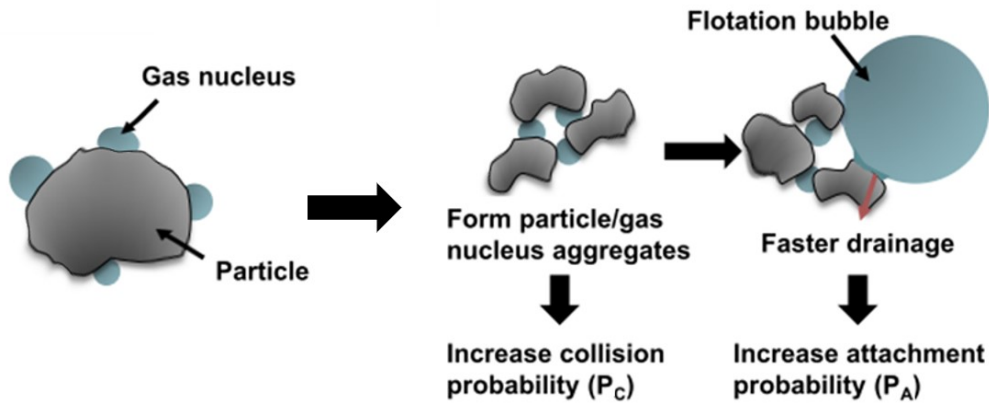


Figure 2-8 Schematic diagram of a two-stage aeration system

In the first stage, micron size bubbles generated by hydrodynamic cavitation selectively on the surface of hydrophobized particles bridge fine particles together, which increases the probability of collision by increasing the apparent size by particle aggregates. In the second stage, such gas nuclei-frosted particle aggregates attach to the flotation size bubbles. Wang et al. (2013) showed that bubble aging greatly affects the bubble-particle attachment. Frothers adsorb on both the surface of micron size bubbles and conventional flotation size bubbles, which increases the induction time of bubble-particle attachment. To avoid the adverse effect of bubble aging on bubble-particle attachment and hence particle flotation, it is highly desirable to generate both micron size bubbles and conventional flotation size bubbles one after another by a dual bubble generator that allows an immediate contact of gas nuclei frosted on desired fine particles and flotation size bubbles.

## 2.4 Design concept of a dual bubble generator

In contrast to hydrodynamic cavitation bubble generator shown in Figure 2-9a which can only generate micron size bubbles, the design of dual bubble generator (Figure 2-9b) is to generate bubbles of two distinct sizes in an attempt to reduce the time between the generation of cavitation bubbles and flotation size bubbles so that bubble aging prior to their contact could be minimized. With such design, the particles frosted with nucleated fine bubbles by hydrodynamic cavitation (G1) are contacted immediately with flotation size bubbles generated by the sintered tube (G2). This design criterion was based on our extensive knowledge accumulated over many years of research that the aging of bubbles increases significantly the bubble coalescence time (Li et al., 2015).

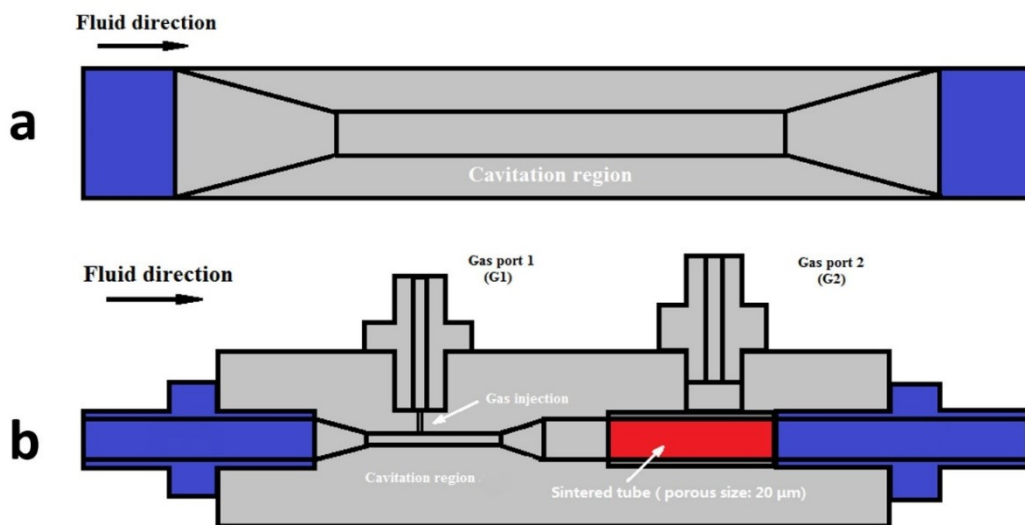


Figure 2-9 Schematics of a hydrodynamic cavitation-based commercial bubble generator (a) and novel dual bubble generator (b)

## **2.5 Hydrodynamic Cavitation**

The hydrodynamic cavitation plays a role in tiny bubble generation. The role played by hydrodynamic cavitation is best explained by mechanical agitation, fast liquid flow, and dissolved gas content processes.

### **2.5.1 Mechanical agitation.**

The method could offer a modest and practical way to generate tiny bubbles without movement in flotation systems. The robust shear prompted by impeller exploit supports the development of bubbles by cavitation in mechanical flotation cells. For instance, miniature bubbles molded close to the agitation region in lab mechanical flotation cell in the presence of added air (Zhou and Chow, 2006). Some may argue that entrained air during agitation leads to the formation of bubbles. Newly heated tap water was tested instantly to determine factors that play part in the formation of cavities. Zhou et al. (2005) noted that much of already existing dissolved gas and gas nuclei in water would have been eliminated. No cavity bubbles could be seen upon cavitation as compared to undeaerated water. This ascertains that air entrainment is not a leading aspect of the formation of cavity effervesce by agitation. Nevertheless, cavity bubbles were observed again upon agitation after the steaming water condensed in a night to equilibrate with the surrounding. In this case, the liquefied air in water moved back to the stability value. It is clear that regardless of already existing gas nuclei, agitation with water saturated with air generated cavity froths was much easier with dissolved air. A given quantity of liquefied gas should be present in the water to thwart the instant breakdown of cavity

froths created by hydrodynamic cavitation.

### **2.5.2 Fast liquid flow.**

To determine aspects impacting hydrodynamic cavitation, systematic experiments by compelling water via a constraint in a flowing stream (Zhou, 1996). A light transmission method was used to detect the formation of bubbles. Zhou et al. (1997) highlighted the critical liquid flow velocity for inception for cavity effervesce did not alter in the presence of a surfactant. However, the presence of surfactant lowered transmittance, indicating an upsurge in the total bubbles formed. An upsurge in the number of bubbles can be due to stabilizing cavities by surfactant adsorption that offer mechanical strength to resist pressure changes (Gogate and Pandit, 2001). Additionally, the presence of surfactant at surface interface could minimize how bubble spurts.

### **2.5.3 Dissolved gas content.**

Profligate liquid flow and agitation can produce voids in water. A given amount of dissolved gases is required to preserve these cavities. Liquefied gas can be directed into the water via dissolving gas under pressure method. Xu et al. (2006) noticed that more froths of reduced sizes were generated from carbon dioxide saturated water than from water saturated with air under HIA by bubbling carbon dioxide and air into de-ionized water for a long time. It is now vivid that gas suspension under pressure is needed for the creation of bubbles in liquefied air flotation, or even procedures including considerably high pressure for comparatively lengthened retention times, say 10 to 20 minutes. Both dissolved gas content and cavity formation in water determine the rate

of generation of bubbles.

## **2.6 Bubble View Analyses**

The photographic techniques are one of the modest methods to investigate bubble dimension in flotation systems. The photographic methods utilized range from photography via transparent walls to imaging of froth. Every capture image, which to fluctuating degrees encompass overlapping, touching, or out of focus froth (Unno and Inoue,1980; Zhou et al., 1993; Yianatos et al.,2001; Polli et al., 2002; Schafer et al.,2002). Image analysis software is utilized to automate the procedure as manual counting confines the total froths. Thus, accuracy depends on image treatment, encompassing filters and counting method. The McGill Bubble size analysis yields single plane, backlight images and uses software that filters by shape factor. It has been proven effective for bubble size distributions stretching from about 0.5mm to 3mm. when the number (D10) and Sauter (D32) mean diameters are compared, consistent trends are observed (Bailey et al., 2005).

## Chapter 3 Experimental Setup and Procedures

There are two different configurations of experimental setup used in this project. The first was used for two-phase flotation tests and is shown in Figure 3-1, and the second was used for three-phase gold flotation tests, which is shown in Figure 3-2.

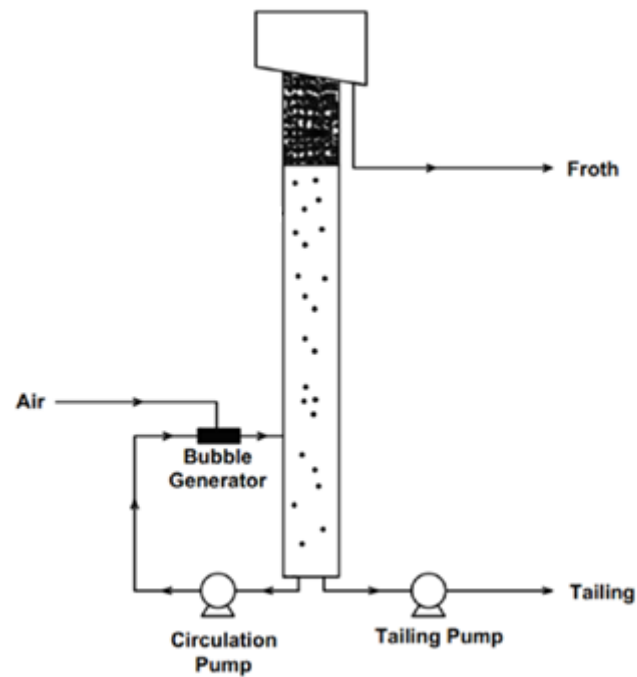


Figure 3-3 Schematics of flotation column used for the two-phase tests

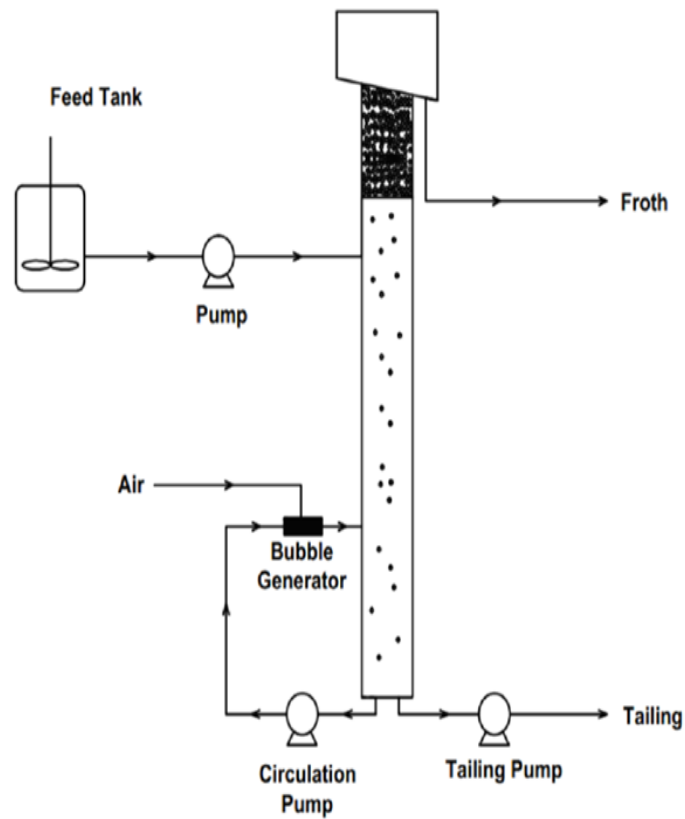


Figure 3-2 Schematics of flotation column used for the three-phase flotation tests of gold ores

### 3.1 Two-phase column flotation test setup

The flotation column as shown in Figure 3-1 for this phase of project was 114.3 cm in height and 10.16 cm inner diameter, corresponding to a total volume of 9.26 L. In order to measure the bubble size, a McGill Bubble View bubble size analyzer was fabricated and introduced into this flotation system shown in Figure 3-3

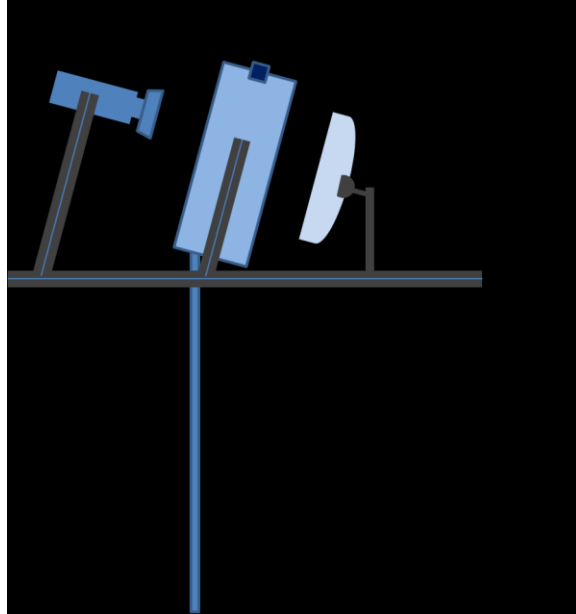


Figure 3-3 Schematics of a McGill Bubble Size Analyzer

The sampling tube was 0.9 m long and 1 cm in diameter (internal) made of plastic materials. The viewing chamber sloped at 15° to the vertical was 30 cm in diameter x 13 cm in width short column constructed of PVC sandwiched between 2 transparent view Plexiglas. The McGill bubble viewer was placed above the flotation column. The sampling tube was inserted inside the column. All the pumps were Masterflex peristaltic pumps. Tygon tubing, supplied by Masterflux, was used to connect the pumps and the column. Bubble size measurements were made using the McGill bubble size analyzer (MBSA) and are reported as the Sauter mean diameter ( $d_{32}$ ). All the tests were conducted at room temperature (25 °C). Before the tests, the circulation pumps were calibrated. The calibration results are shown in Figure 3-4. The flow calibration done with tap water, in Masterflex 06401-82 yellow tubing.

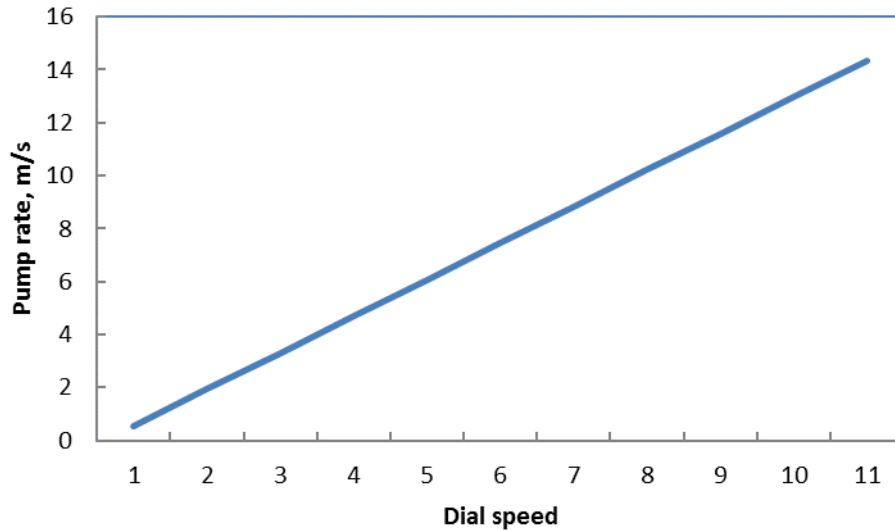


Figure 3-4 Calibration chart of pumps

In order to test the performance of dual bubble generator, the gas holdup in different conditions was measured by manometer. To measure the gas holdup, either pressure difference or conductivity probes can be used. In this thesis, the pressure difference method by monometer was used for the gas holdup measurements. It should be noted that the gas holdup is not uniform across the cross section of the flotation column. In the center of the column, the gas holdup is higher than that near the wall of the flotation column (Tavera et al., 2001). For this study, the column inner diameter is 4 inches, which only has little affected on gas holdup distribution. A schematic of monometer is shown in Figure 3-5 and the gas holdup calculative process is shown as:

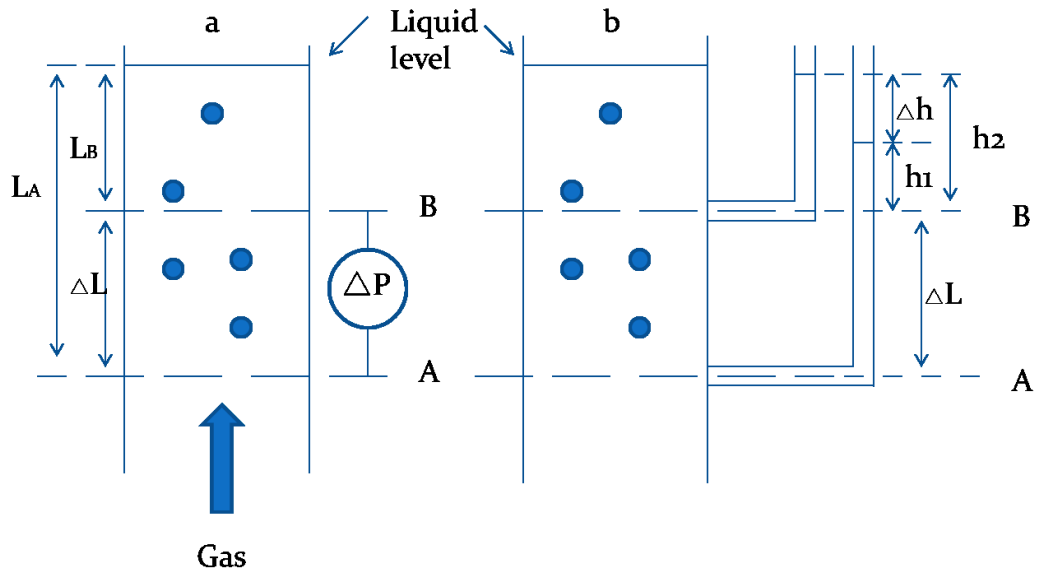


Figure 3-5 Measurement of gas holdup by pressure difference: (a) General and (b) using water monometer

The pressure on location A and location B defines as:

$$P_A = \rho_{sl} g L_A (1 - \epsilon_A) \quad (3)$$

$$P_B = \rho_{sl} g L_B (1 - \epsilon_B) \quad (4)$$

where the  $P_A$  and  $P_B$  is the pressure at location A and location B,  $\rho_{sl}$  is the density of the slurry in the column,  $g$  is the gravitational acceleration,  $L_A$  is the vertical distance between point A and water level,  $L_B$  is the vertical distance between point B and water level,  $\epsilon_A$  and  $\epsilon_B$  are the average volume fraction of gases up to these two locations.

The pressure difference between A and B is given by:

$$\Delta P = P_A - P_B = \rho_{sl} g \Delta L (1 - \epsilon_g) \quad (5)$$

where  $\epsilon_g$  is the volume fraction of gas (air) between points A and B in the column.

Since the pressures at points A and B are equal to those in the corresponding legs of the manometer, we have:

$$\Delta P = \rho_{sl}g[(\Delta L + h_1) - h_2] \quad (6)$$

where  $\Delta h$  is the manometer reading. Equations 5 and 6 can be combined to obtain

$$\rho_{sl}g\Delta h(1 - \epsilon_g) = \rho_{sl}g(\Delta L - \Delta h) \quad (7)$$

Equation 7 can be rearranged to become:

$$\epsilon_g = \frac{\Delta h}{\Delta L} \quad (8)$$

Finally, the gas holdup can be calculated using Equation 6 through measured  $\Delta h$  and  $\Delta L$ .

However, gas holdup does not give directly the size of the bubbles in the column. This is why the bubble size measurement system (bubble view) is built. In a typical experiment, the viewing chamber is filled with water with the top valve being closed and the sampling tube being inserted into the flotation column. Due to atmospheric pressure, the water level in the viewing chamber remains unchanged and the water in the chamber will not return from the sampling tube to the flotation column. If bubbles appear in the flotation column, the bubbles will be sampled and rise into the viewing chamber along the sampling tube due to buoyancy force. Because there are  $15^\circ$  angle between the viewing chamber and the vertical plane, bubbles in chamber can rise and slide along the inclined plane. This manner avoids the stack of bubbles, making the image clearer and easier to be viewed. The number and the size of bubbles were monitored using a high-speed camera equipped with a high magnification lens. A back light was used from the back of the chamber to provide enough and uniform light intensity for clear imaging. Using the MATLAB software, we can analyze the obtained

images and obtain the size of the bubbles in the images (MATLAB code for imaging analysis is given in the appendix).

After the pictures are made, they are analyzed on the computer. The bubbles must be identified, and their diameter determined. The four steps that are followed in bubble size measurement from stilled images are shown in Figure 3-6. The first step is to select the image we want to analysis and convert it grey scale. The contrast of the image is then enhanced to make the edges clear. A specified threshold value is used to obtain a binary image where only the edges are left, because of the lowest intensity of the edges. Depending on the size of the bubbles, between 85-95% of the bubbles on each image are found correctly. The last step is to find the circle and count the number and corresponding diameters of the bubbles shown in the photo.

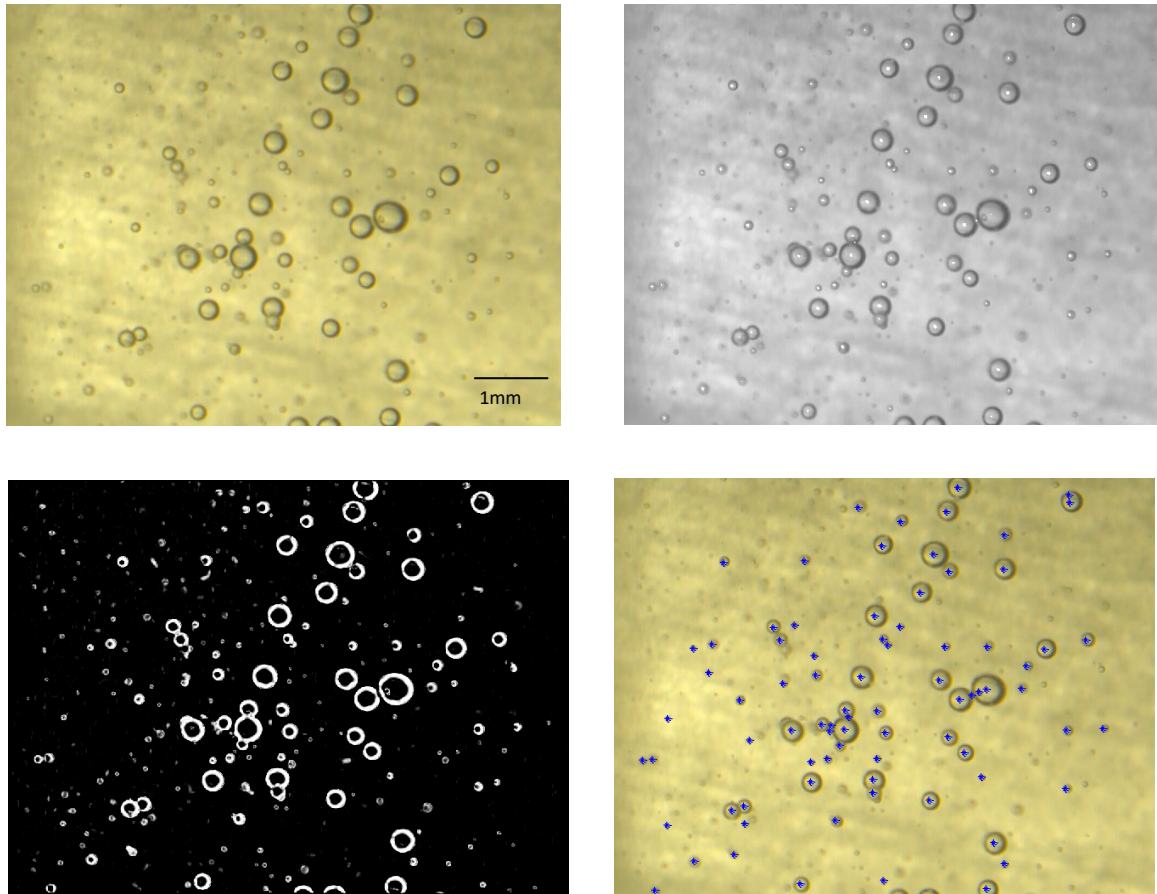


Figure 3-6 Original image of bubble (Top left), the image transformed to grey scales (Top right), image made into binary by a thresholding value while keeping the edges (Bottom left), find the circles (Bottom right), and count the number and calculate the average diameter of bubbles

### 3.2 Two-phase column flotation test methods

The tap water with 10 ppm and 20 ppm MIBC (methyl isobutyl carbinol) aqueous solutions was used in this project. The frother was mixed with the tap water in a tank under agitation for 45 seconds. After filling the column with the prepared frother solutions (emulsions), the tailing pump was reversed to fulfill the bubble viewer chamber. air at the controlled volumetric flow rate was then injected into the dual bubble generator through gas port 1 and/or gas port 2 (G1 and G2, respectively) while

the bubble sliding in the bubble view is recorded. To stabilize the column operation and obtain accurate results, the data were collected after the flotation column reaching the steady state. The gas holdup was measured by the monometer and bubble size measured using images recorded by McGill bubble viewer.

### **3.3 Three-phase column flotation setup**

An introduction of equipment used in the program, head material (chemical analysis and mineralogical investigations) and reagents applied for column flotation is given below. A laboratory size column with an inner diameter of 0.076 m and height 1.32 m was used in this study. Two gas flow meters were installed to measure the injection rates of gas to dual bubble generators during the flotation tests. Pulp circulation rate, feed rate, tailings withdraw rate and the frother addition rate were controlled by four different peristaltic pumps. One 50-L tank with an overhead agitator was used for mixing the slurry. As shown in Figure 3-1, the bubble generator was installed between the column and the circulation pump. As a comparison, a commercial bubble generator was used in the same column flotation system. The following experimental parameter were used during the three-phase column flotation tests.

#### **Head Material**

The Goldstrike BR20 ore was tested in this program. It is a double refractory ore with 3 g/t Au, 1.5% TCM (organic carbon) and 0.7% sulfide. The head assay for BR20 is shown below.

Table 3-1 BR20 head assay

Sample	Au	C total	C org	C inorg	S total	S <sup>2-</sup>	S <sub>SO4</sub>
	g/t	%	%	%	%	%	%
BR20	2.97	5.41	1.54	3.87	1.02	0.69	0.33

Table 3-2 BR20 ore modal mineralogy

Modal Analysis	
Mineral Abundance	BR-20 Composite
Chalcopyrite	1.69
Arsenopyrite/Realgar	0.00
Sphalerite	0.08
Iron Oxides	0.95
Quartz	57.14
Muscovite	5.11
K-Feldspars	1.03
Dolomite	25.31
Calcite	3.25
Ankerite/Siderite	0.14
Ca-sulphate	0.06
Plagioclase Feldspar	0.19
Chlorite	1.02
Pyroxene	0.29
Kaolinite	1.02
Apatite	0.22
Rutile/Anatase	0.30
Barite	0.14
Zircon	0.03
Organic Carbon	1.75
Others	0.21
Total	100.0

Previous mineralogical investigations revealed that gold was mainly locked within

pyrite and that some of the gold was also associated with TCM (Total carbonaceous matter). Most of the gold is in sub-micron size and in the form of solid solution gold.

Other mineralogical features include:

- i. The bulk mineralogy of BR-20 ore was mainly composed of quartz (57.1%) and dolomite (25.3%) with minor amounts of calcite, chlorite, mica, feldspar and kaolinite.
- ii. A minor amount of pyrite (1.69%) and less than 1% of goethite were noted. Morphologically, most of the pyrite grains were porous, fine and micro-crystalline/disseminated pyrite aggregates. Both massive goethite and fine/disseminated goethite were noted.
- iii. A minor amount of TCM (1.75%) was found.
- iv. Pyrite liberation (>95% liberated) was 43%. The majority of the goethite was liberated.
- v. 21 components of gold grains were noted in the BR-20 composite sample. All were native gold with Au content ranging from 86% to 100%. The majority of gold grains found were liberated and fine to medium grained (5  $\mu\text{m}$  to 12  $\mu\text{m}$ ). A few locked grains in sulfides and silicates were also noted.

### **3.4 Three-phase column flotation test procedures**

The BR20 ore was first ground to P<sub>80</sub> of 25 $\mu\text{m}$  using a pilot rod mill. The slurry was then diluted to 20 wt% solids in a 50-L conditioning tank. PAX (Potassium amyl

xanthate) and S-10351 (Pine oil) as the collector were introduced to the conditioning tank and the resultant slurry was conditioned for 10 minutes. A mixture of 3:1 MIBC/DF250 was emulsified in the tap water and be used as the frother. The frother emulsion was pumped at a desired volumetric flow rate to the feed entering the column. For a selected number of tests, wash water was added from the top of the column. Air at the controlled volumetric flow rate was injected into the dual bubble generator through gas port 1 and/or gas port 2 (G1 and G2, respectively). For the commercial bubble generator, air was injected from the gas cylinder directly into the bubble generator. In this study, the flotation time at each pulp condition was fixed at 20.5 minutes. The concentrate and tails were collected for analysis after the first 20 minutes of continuous running of the flotation in the column to ensure the system to reach the steady state when starting a new flotation test or changing flotation test conditions. The pictures of mineral concentrate and tailings are shown in Figure 3-7. For comparison, flotation tests were conducted using two different bubble generators (dual bubble generator and the commercial bubble generator) in the same column flotation system. A selected number of tests were also conducted using a mechanical flotation cell (Denver flotation cell) with the identical flotation pulp chemistry.

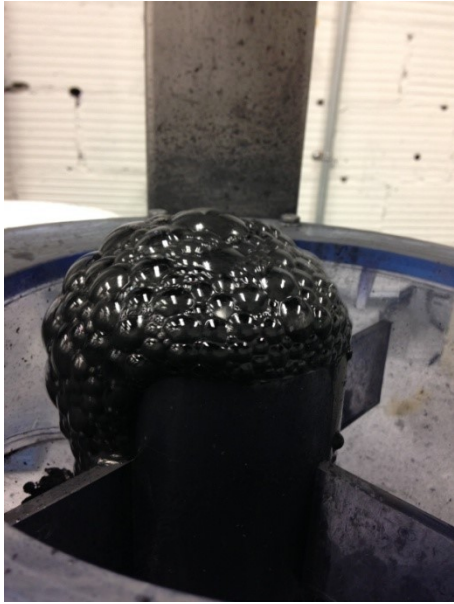


Figure 3-7 Flotation concentrate (Left) and tailings (Right) of BR20

## **Chapter 4 Experimental Results and Discussion**

### **4.1 Two-phases column flotation tests**

#### **4.1.1 Bubble size**

The water-gas two-phase tests were conducted with tap water with and without MIBC (methyl isobutyl carbinol).

##### **(1) Effect of gas injection location on bubble size**

It is important to investigate whether the hydrodynamic cavitation-based dual bubble generator can generate both micron size bubbles and flotation size bubbles during the tests.

In this section, the size of bubbles generated by the dual bubble generator in water at different gas injection rates through different ports was determined. One typical image of gas bubble distribution when only injecting gas through G1 port is shown in Figure 4-1. The typical image of gas bubble distribution when only injecting gas through G2 port is shown in Figure 4-2. When injecting gas through both G1 port and G2 port, the typical image is shown in Figure 4-3.

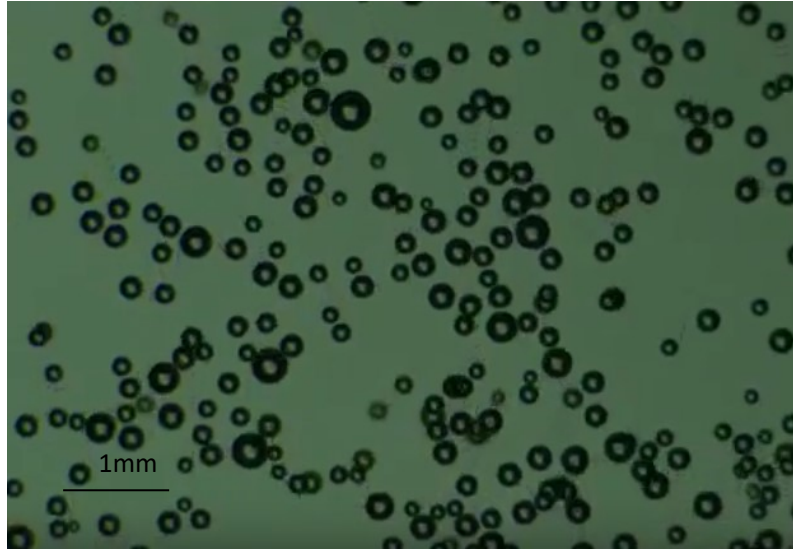


Figure 4-4-1 Bubbles of air injected only from G1 ( $G_1=2$  L/min,  $G_2=0$  L/min, Throat velocity at 8 m/s, MIBC concentration is 10 ppm)

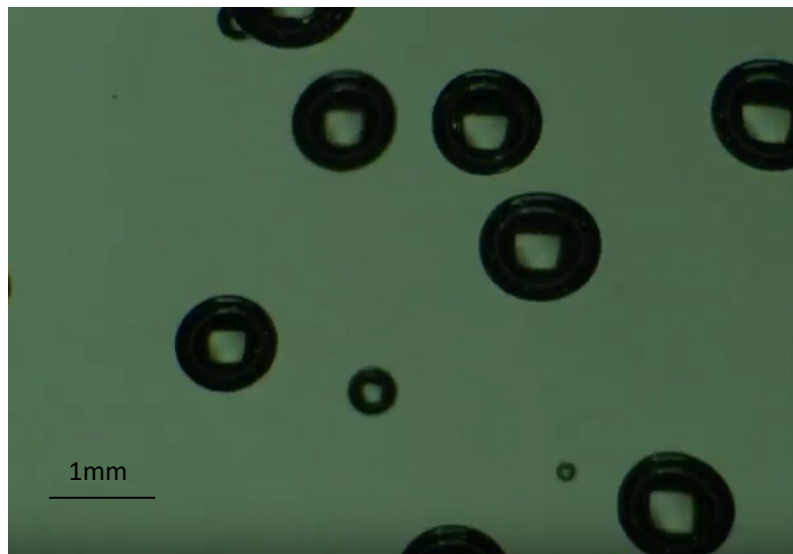


Figure 4-1-2 Bubbles of air injected only from G2 ( $G_1=0$  L/min,  $G_2=2$  L/min, Throat velocity at 8 m/s, MIBC concentration is 10 ppm)

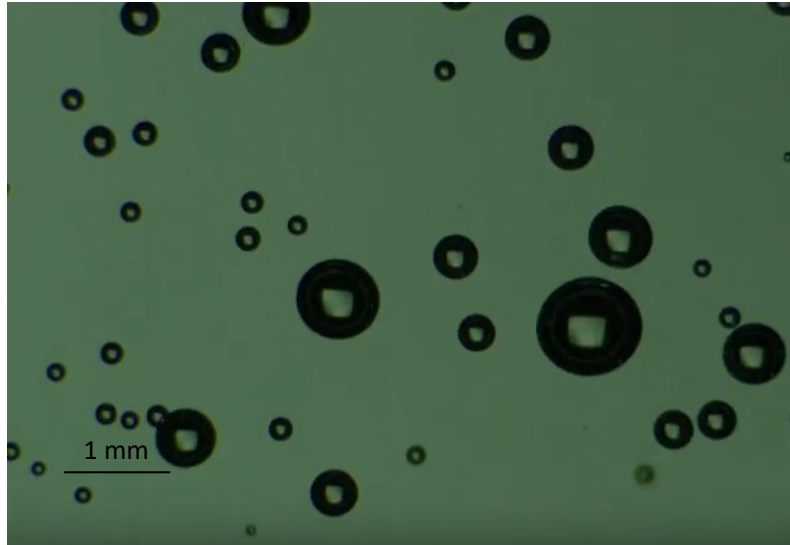


Figure 4-1-3 Bubbles of air injected from G1 and G2 (G1= 1 L/min, G2=1 L/min, Throat velocity at 8 m/s, MIBC concentration is 10 ppm)

Based on the design concept, micron size bubbles are generated from air injected at point G1, while the flotation size bubbles are generated from air injected at point G2. Figure 4-1-1 shows that most of bubbles are small, which are generated by injecting air through port G1 only. If the air is injected through G2 port only, large bubbles are generated in the flotation column. If air is injected through both ports G1 and G2, it is clearly from the Figure 4-1-3 that both large bubbles and small bubbles are present in the flotation column as anticipated.

The results in Figure 4-1-4 are obtained with 10 ppm MIBC addition into the flotation system and air injected through port G2. The smallest size of bubbles is 0.08 mm, and the largest size is 1.01 mm. The average size of bubbles is 0.43 mm. The figure shows that most of the bubbles are in the size range between 0.38 mm to 0.44mm.

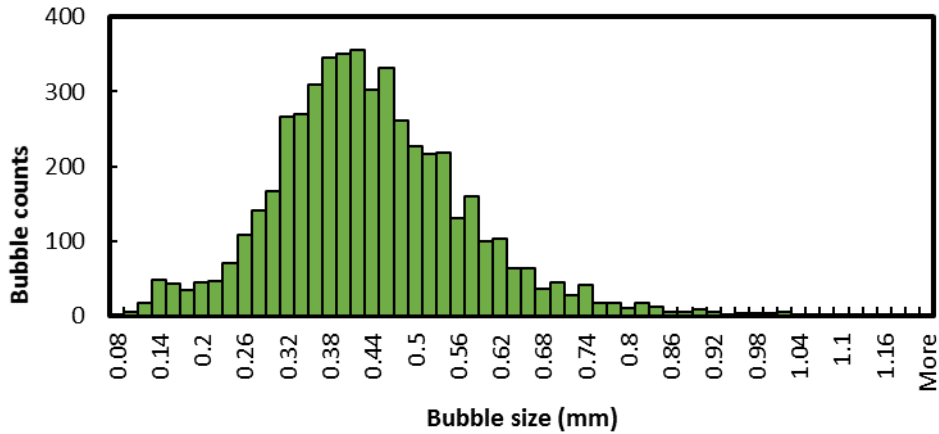


Figure 4-1-4 Effect of air injection through G2 on bubble size (G1= 0 L/min, G2=2 L/min, Throat velocity at 8 m/s, MIBC concentration is 10 ppm)

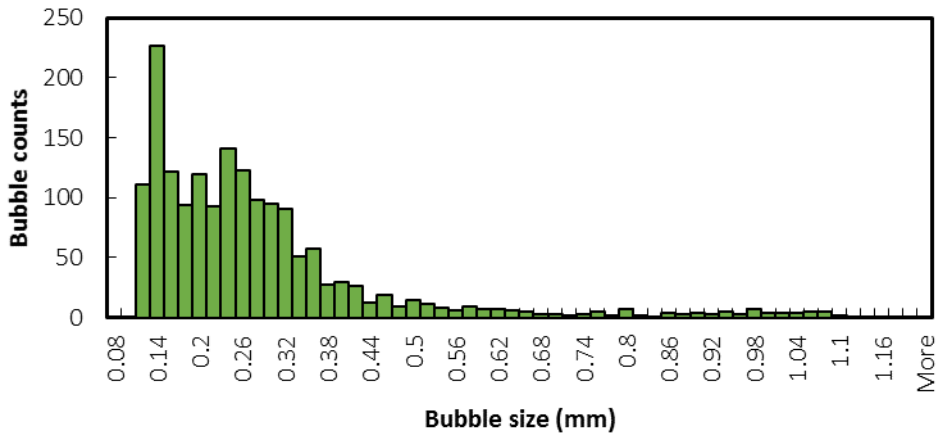


Figure 4-1-5 Effect of air injection through G1 on bubble size (G1= 2 L/min, G2=0 L/min, Throat velocity at 8 m/s, MIBC concentration is 10 ppm)

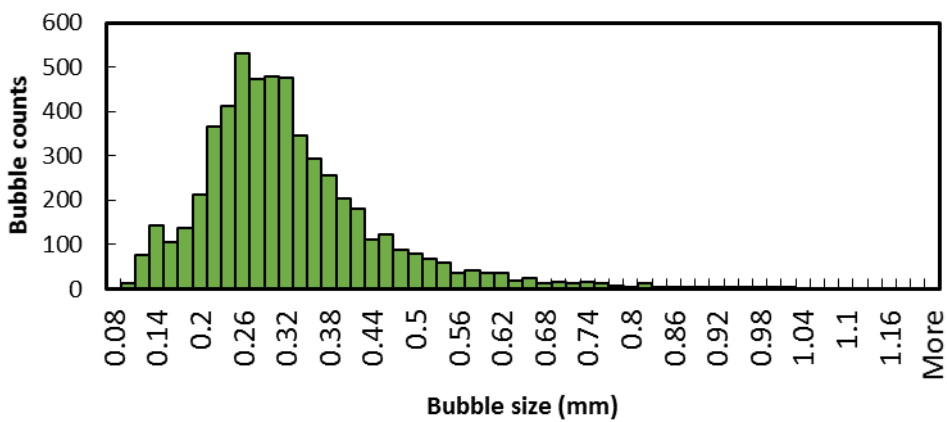


Figure 4-1-6 Effect of G1 and G2 on bubble size (G1= 1 L/min, G2=1 L/min, Throat velocity at 8 m/s, MIBC concentration is 10 ppm)

In this flotation system, 10ppm MIBC was added into the flotation system, shut the G2 port, inject the airflow through G1. As shown in figure 4-1-5, the smallest bubble diameter is 0.10cm and the largest is 1.09 mm. The average size of gas bubbles is 0.27 mm. The figure shows that most bubbles are between 0.26 mm and 0.36 mm. The most bubbles are 0.14 mm. In the same flotation conditions, if we inject gas through G1 port and G2 port at the same time, the average bubble size is 0.32 mm. Comparison the results from Figure 4-1-4, 4-1-5 and 4-1-6, we can found that under the same flotation conditions, the gas bubbles generated from G1 port have smaller size than injecting gas though G2 port. Two different sizes of bubbles will be generated when inject the gas through G1 port and G2 port at the same time. The results are also consistent with the results of gas holdup.

## **(2) Effect of gas injection rate on bubble size**

Gas injection rate is a variable of major importance in flotation kinetics, and it is used as a control or optimization variable in some flotation plants (Manlapig and Spottiwood, 1978; Neimi and Paakkinen, 1969). In this section, the size of bubbles generated by hydrodynamic dual bubble generator in water at different gas injection rate was determined. Figure 4-1-7 shows the bubble size as a function of gas injection rate at different gas injection ports.

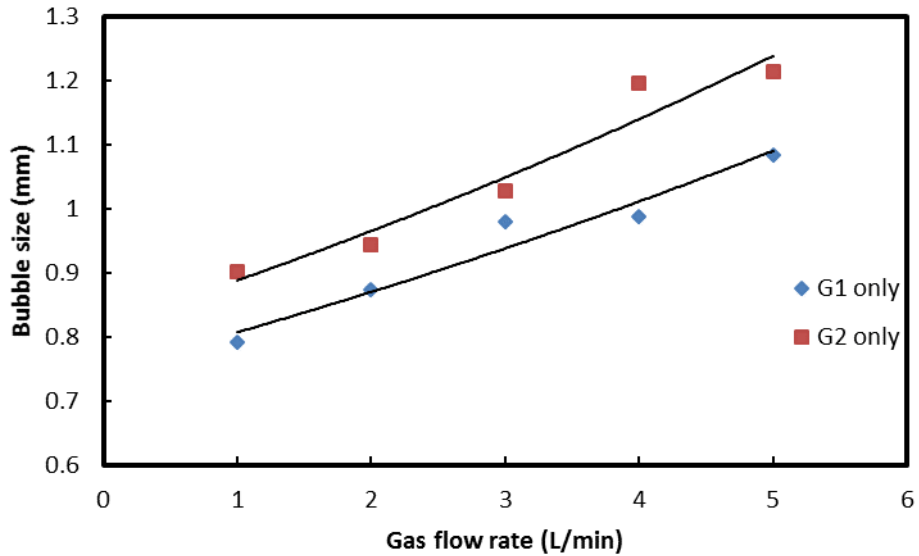


Figure 4-1-7 Effect of gas injection rate on bubble size (G1=1L/min, G2=0L/min)

The Figure 4-1-7 shows that the bubble size increased with increasing the gas injection rate from 0 L/min to 5 L/min. As demonstrated above, small bubbles are generated when gas injected from G1, while big bubbles are generated when gas injected from G2. The trend line from G1 is lower than G2. In this test, no frother was added into the test. In that case, the bubble size is much larger than the bubble size we measured before (with frother).

### (3) Effect of frother on bubble size

In order to reduce the bubble size, the frother MIBC was introduced to the column test. In this section, the size of bubbles generated by hydrodynamic dual bubble generator in water at different frother concentration was determined.

Comparison of bubble sizes in 0 ppm MIBC solution, 10 ppm MIBC solution and 20

ppm MIBC solution were shown in Figure 4-1-8. As noted in Figure 4-1-8, bubble size decreased significantly with increasing MIBC concentration from 0 ppm to 20 ppm at air injection rate ranges from 1L/min to 5 L/min. Addition of the frother prevents the bubble coalescence as well as the bubble deformation. Thus, the bubble size decreases with increasing the frother concentration. However, the bubble size difference between 0 ppm and 10 ppm is much higher than 10 ppm to 20 ppm. This is due to the addition of frothers with concentration lower than their critical coalescence concentration (CCC) led to quick decrease in bubble size (Melo, 2001; Nasset et al. 2006 and Finch et al. 2008). On the other hand, adding frothers concentration with higher than CCC decrease bubble size slowly.

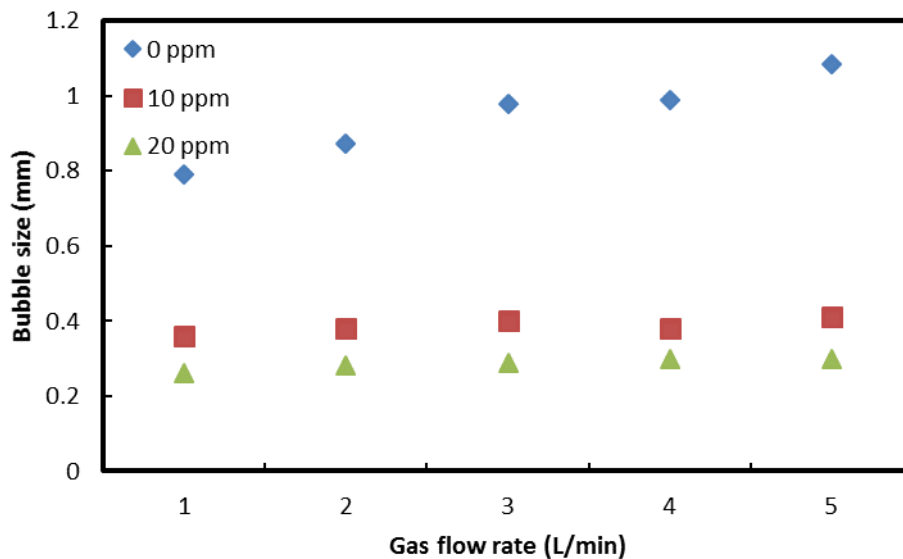


Figure 4-1-8 Effect of MIBC concentration on bubble size (G1=1L/min, G2=0L/min)

#### 4.1.2 Gas hold up

To confirm the benefit of fresh bubble coalescence, water/air two-phase system was investigated. Although it is more informative to determine the size of bubbles generated

by dual bubble generator, we determined gas holdup as a measure of bubble generation in flotation column due to its simplicity of measurement. Gas holdup was calculated from measured pressure differential between two reference points along the column.

### **(1) Effects of airflow rate on gas holdup**

In this section, the gas holdup in water/air system at various airflow rates was determined. Figure 4-1-9 shows the gas holdup as a function of airflow rate at different gas injection ports. As shown in Figure 4-1-9, the gas holdup in the flotation column increases as the rate of gas injection increases. In this set of experiment, no MIBC was added into the flotation column, only water and air. In the absence of air injection, the rate of the circulating pump has reached cavitation speed, and hydrodynamic cavitation happens in the throat of the bubble generator. The section area of the throat is less than the area of the fluid inlet. According to Bernoulli's theorem, the fluid velocity increases with decreasing the cross area of the tube, while the pressure decreases with decreasing the cross-section area in the throat. When the pressure is less than the vapor pressure, gas nuclei will be formed. This creates micro bubbles. The formation of bubbles in flotation columns can be expressed by gas holdup. To sum up, gas holdup is about 1% without any gas injected into the column. As the gas is injected from G1 and G2 ports, the gas holdup in the flotation column increases with increasing the gas flow rate. As shown in the figure, under the condition of the same amount of gas flow rate (L/min), the gas holdup value measured from injecting gas through G1 port is higher than injecting gas through G2. When the gas injection rate was 5 L/min, the gas holdup alone from G1 gas injection was 8%, while the gas holdup alone from G2 gas injection was

6%. Based on the design concept of dual bubble generator, the gas injected from G1 port directly goes into the throat of the bubble generator, which can help to increase cavitation efficiency and to generate micron size bubbles. The gas injected from G2 port forms big bubbles through the mesh screen in the outlet the bubble generator. The size of gas bubbles generated from G1 port is smaller than which generated from G2 port. The small bubbles buoyancy velocity is less than the floating rate of large bubbles due to the different size between small bubbles and large bubbles. Therefore, in the same amount of gas, the gas holdup of the G1 injection only is higher than that of the big bubbles.

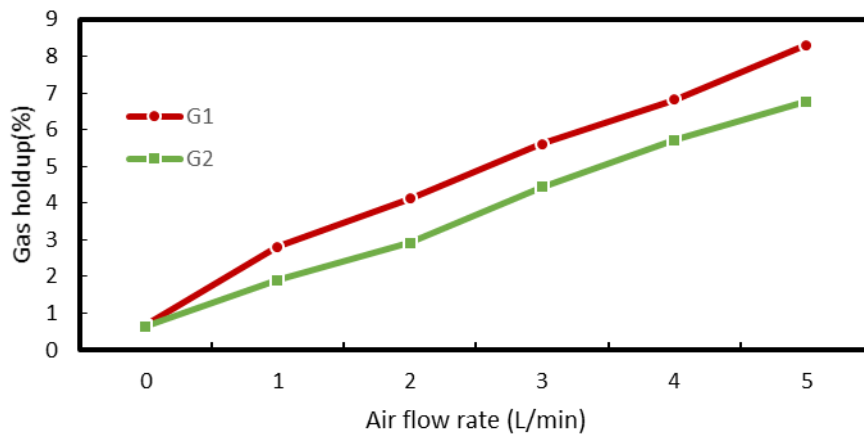


Figure 4-1-9 Gas holdup as a function of air flow rate, which injected at G1 and G2, respectively

**(2) Effect of MIBC concentration on gas holdup with G1, G2**

In this section, the gas holdup in water/air system at various frother concentrations was determined. Figure 4-1-10 shows the gas holdup as a function of airflow rate at different gas injection ports with 10 ppm MIBC added. Figure 4-1-11 shows the gas holdup as a function of airflow rate at different gas injection ports with 20 ppm MIBC added. Figure 4-1-12 shows the gas holdup as a function of MIBC concentration at the same gas

injection rate. As shown in Figure 4-1-10 and 4-1-11, gas holdup varies at different MIBC concentration. With 10ppm MIBC in flotation, gas holdup reached 16% maximum at G1 injection only. Gas holdup maximum was 9% at G2 injection only. With 20ppm MIBC in flotation, gas holdup was maximum 28% at G1 injection only. Gas holdup was maximum 13% at G2 injection only. As shown in Figure 4-1-12, gas holdup increases with increasing the MIBC concentration.

High gas holdup represents high concentration in flotation. Bubbles are crucial factor in mineral flotation. Rising bubbles carry hydrophobic mineral particles from pulp to the surface and purify further in foam layer to high quality concentrate. As mentioned above, bubble size affects flotation efficiency. Compared with micro bubbles, the large bubbles have smaller surface area, few particles can be floated per cubic meter air. Too small diameter bubbles carrying full particles cause average density of mineral bubbles lower than pulp density, thus bubbles cannot float to surface, which influence flotation efficiency. Bubble coalescences in fine particle flotation also influence the flotation efficiency. For above reasons, flotation agent is used in flotation to endure bubbles life and size. From thermodynamics view, bubble is a system of large surface area. Compare with system with no bubbles, minimum free energy of surface area secure stable system. Frother offers orientation arrange at bubble surface to direct polar group towards water, which slow down water to vaporization or bubble specific gravity drop to downstream. All that makes it difficult for bubble wall collision to happen. Flotation agent molecule arranges orientation at bubbles surface so that bubbles will not be merged when collision happened. Tiny bubbles are easier to be kept. Helped by frother, tiny bubbles

generated by injected gas from G1 port are stable. As shown in Figure 4-1-11, gas holdup increased tremendously as frother added at the same gas injection rate from G1 and G2 port.

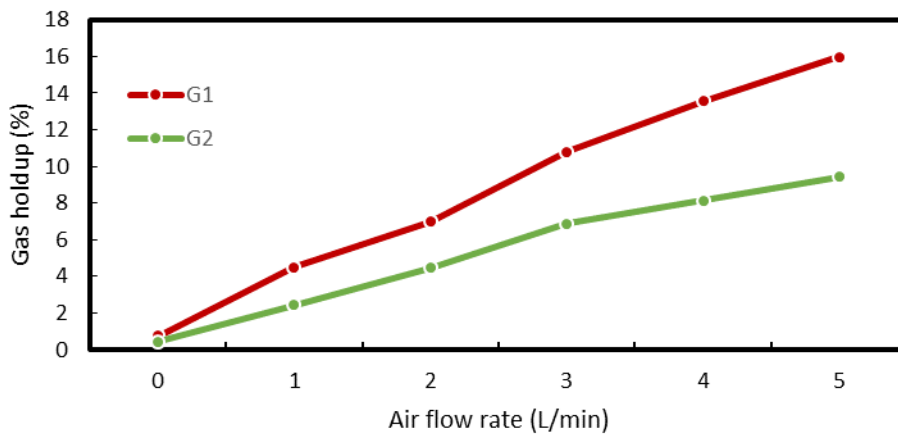


Figure 4-1-10 Gas holdup as a function of air flow rate which injected at G1 and G2, respectively with 10 ppm MIBC added

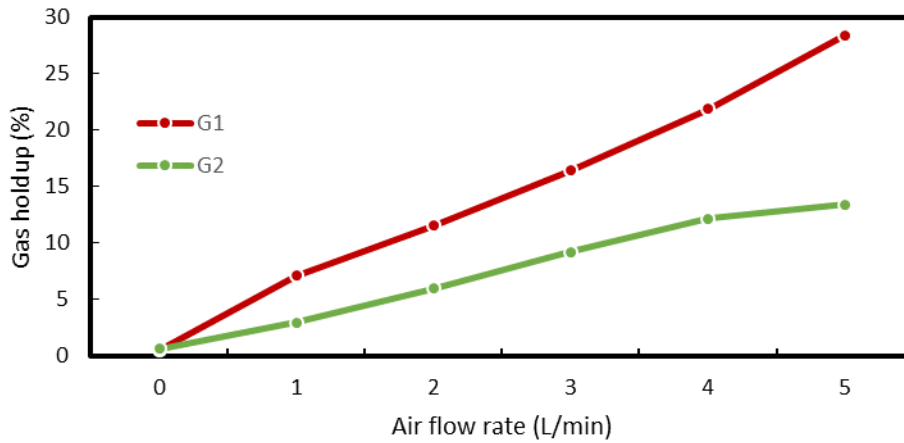


Figure 4-1-11 Gas holdup as a function of air flow rate, which injected at G1 and G2, respectively with 20 ppm MIBC added

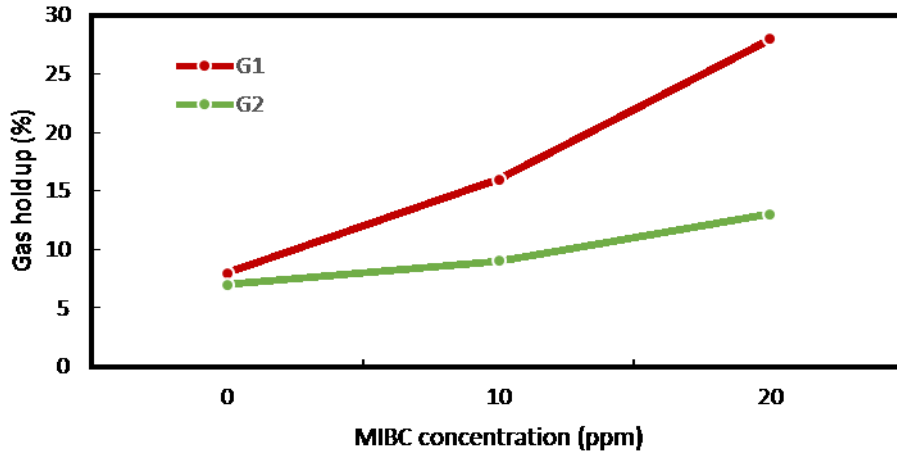


Figure 4-1-12 Effect of MIBC concentration on gas holdup

### (3) Effect of gas port on gas holdup

In this section, the gas holdup in water/air system at various gas injection points was determined. Figure 4-1-13 shows the gas holdup as a function of gas flow rate at G1 gas injection port. Figure 4-1-14 shows the gas holdup as a function of gas flow rate at G2 gas injection port. The gas holdup in water/air system at MIBC concentration from 0 ppm to 20 ppm is reported both in Figure 4-1-13 and Figure 4-1-14. The gas holdup increased with increasing the injection of gas through G1 as shown by the symbols in Figure 4-1-13. However, the overall gas holdup is lower than the additive values shown by the solid line of the figure. The gas holdup difference between the additive values and measured values decrease with increasing the MIBC concentration. This finding indicates significant coalescence of fresh cavitation bubbles generated by G1 with flotation size bubbles generated by G2, as designed for the current purpose.

The gas holdup increased with increasing the injection of gas through G2 as shown by the symbols in Figure 4-1-14. However, the additive values of gas holdup is higher than

measured gas holdup. The gas holdup increases with increasing the froth concentration and increasing the gas injection rate from G1 and G2 port.

Comparison of the Figure 4-1-13 and 4-1-14, the gas holdup difference between measured values and additive values decrease with increasing the froth concentration. However, the gas holdup difference decreases faster from G1 port than G2 port. Thus, G1 dominates the gas holdup in this flotation system.

It is an approximately linear increase in gas holdup with increasing the gas rate, which is shown in Figure 4-1-13 and 4-1-14. However, when the total gas flow rate exceeds 8 L/min, the gas holdup decreases with increasing the gas flow rate. Fuerstenau et al., point out that the linear section is "bubbly flow", which is characterized by fairly uniform sized bubbles. The "churn-turbulent" flow led to the gas holdup decrease. In churn-turbulent flow, the gas injection rate has exceeded the mechanism's ability to disperse the air, which led to form the large bubbles. These large bubbles rise rapidly and displace the fluid and micron bubbles downward.

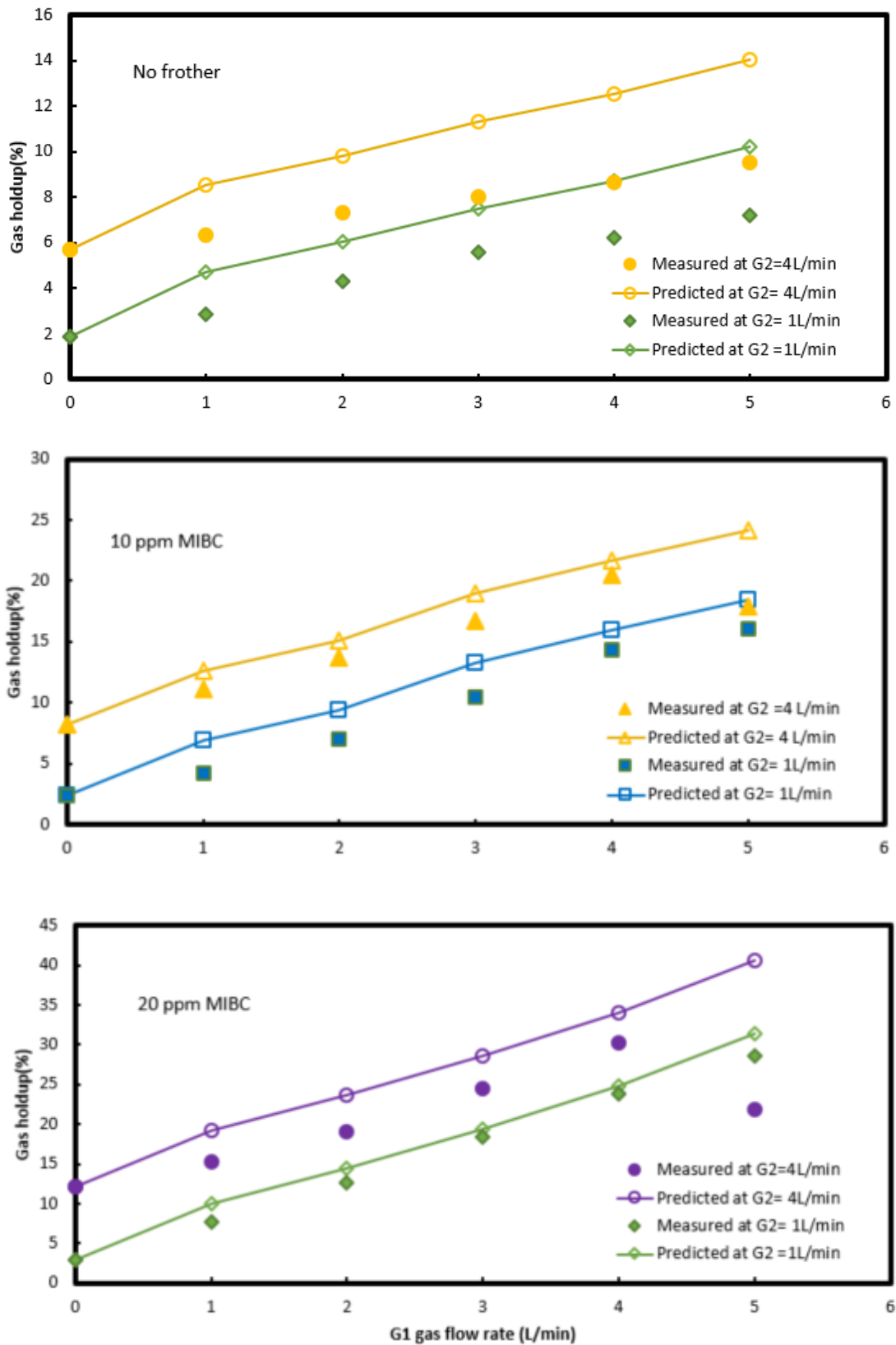


Figure 4-1-5 Effect of variation in gas flow rate in G1 on increase in overall gas holdup

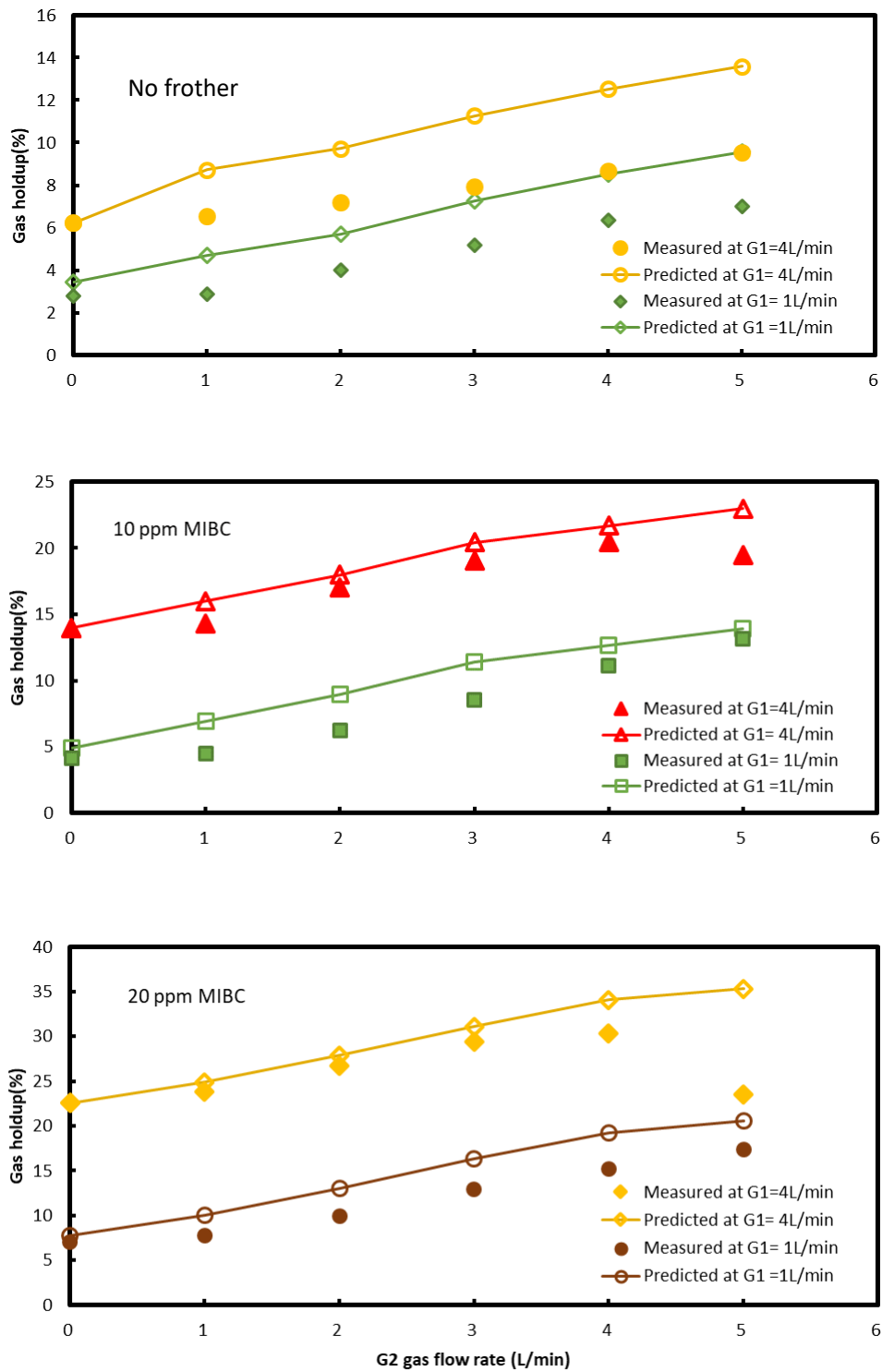


Figure 4-1-14 Effect of variation in gas flow rate in G2 on increase in overall gas holdup

## 4.2 Three -phase column flotation tests

To demonstrate the value of hydrodynamic cavitation based dual bubble generator in recovering fine particles, the flotation tests were conducted using a Nevada double refractory gold ore.

### 4.2.1 G1, G2 injection rate

As shown in Figure 4-2-1, when G2 air flow increase from 0 L/min to 2.5L/min, concentrate yield and recovery increased tremendously. However, when airflow goes over 2 L/min, it shows a pool separation performance for gold and TCM. Gold grades drops from 8.35 g/t to 5.27 g/t, TCM percentage in concentrate drops from 5.58 g/t to 3.47 g/t. Therefore, G2 airflow performs the best airflow rate as 2L/min.

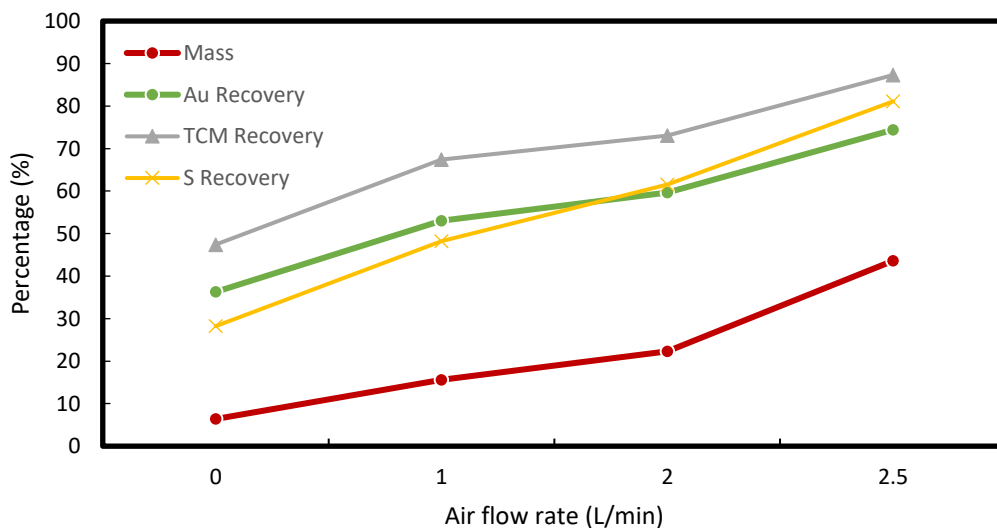


Figure 6 G2 Air flow rate vs mass and recovery

After the amount of air injection of G2 is determined, adjust the amount of G1 air injection of G1 from 0 L/min to 1.5 L/min. As shown in Figure 4-2-2, both the yield and recovery increase with flow rate increase of the injected gas.

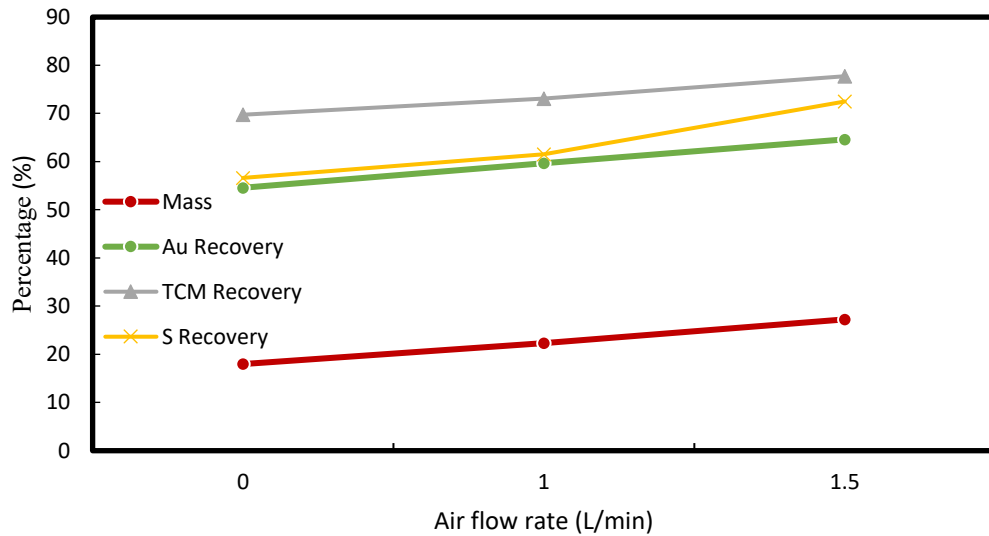


Figure 4-2-2 G1 Air flow rate vs mass and recovery

#### 4.2.2 Froth depth

The increase of foam layer can enhance the secondary enrichment of foam and improve the selectivity of flotation. However, when the level of the flotation column is fixed, the increase of the foam layer thickness leads to the decrease of height of the trap area and the reduction of the recovery rate. When the thickness of the foam layer is too thick, it is easy to cause the overflow of the foam bottom concentrate to be blocked.

Column level is defined as the distance from the level sensor to the point at which the froth starts to form. A long column level always reflects a low froth depth. As shown in Figure 4-2-3, Recovery increased with decreasing the froth depth. Low froth depth led to low selectivity of the flotation.

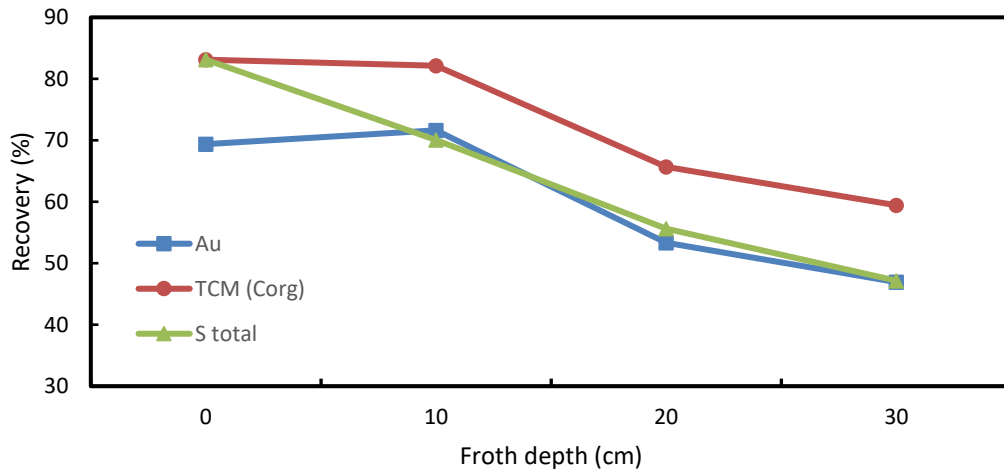


Figure 4-2-3 Froth depth vs mass and recovery

### 4.2.3 Cavitation pump circulating rate

The cavitation pump used to circulate slurry to enable solids to have more than one chance of being floated to concentrate, thereby increasing recovery. However, a high circulating load also reduces column residence time, thereby reducing particle collection probability. As shown in Figure 4-2-4, when cavitation pump circulating rate increases from 5.1 m/s to 6.3L/s, both mass pull and recovery percentage increase.

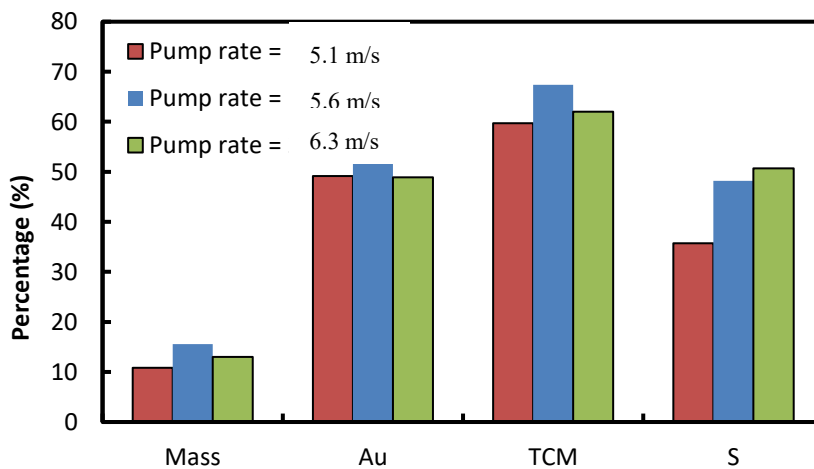


Figure 7 Circulating flow rate vs. mass and recovery

#### 4.2.4 Comparison of Long and short column using the dual bubble generator

During column flotation, a long flotation column is selected for a long residence time of particles. However, only long residence time of particles does not always lead to the increase in recovery percentage. Too long flotation column not only increases the cost of operation, but also may affect the recovery percentage. Therefore, the height of the flotation column is also an important factor for mineral flotation. As shown in Figure 4-2-5, Figure 4-2-6 and Figure 4-2-7, dual bubble generator has better performance on a short flotation column. This can not only reduce the cost of production, but also increase the recovery of minerals and improve the efficiency of flotation. Compared with long flotation column, the recovery rate of gold is increased by 5%, and the recovery rate of sulfur is increased by 20% when a short flotation column is selected. The recovery of TCM is not improved obviously.

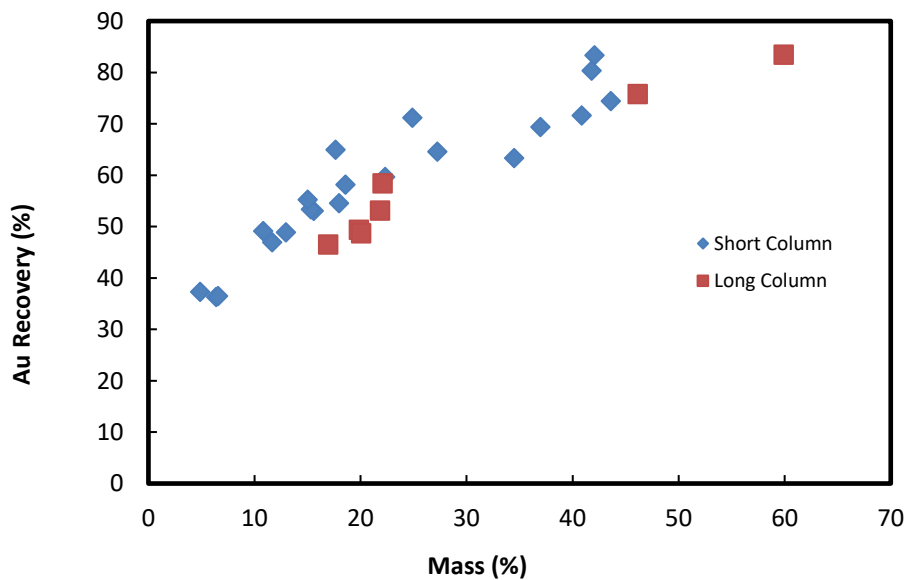


Figure 4-2-5 Au recovery vs mass pull for short and long column

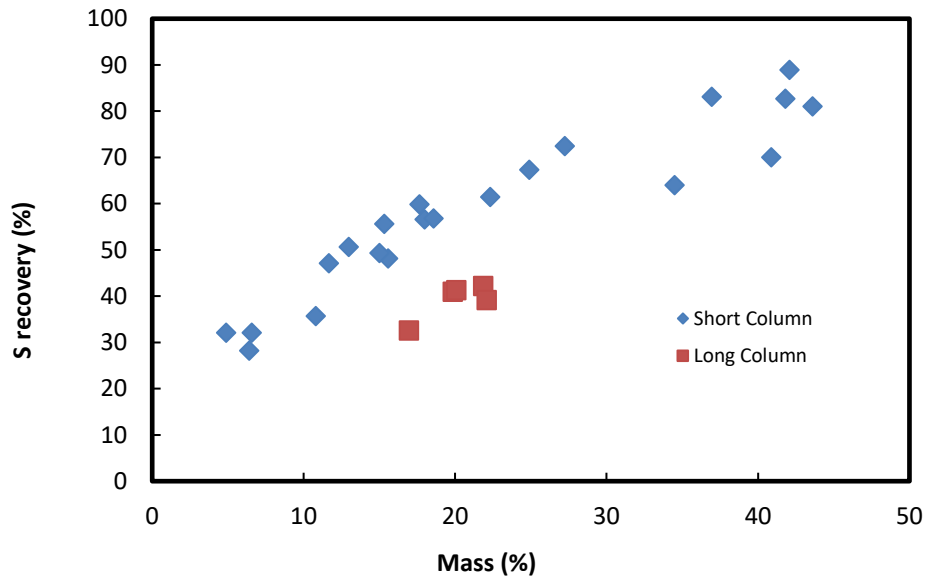


Figure 4-2-6 Sulfide recovery vs mass pull for short and long column

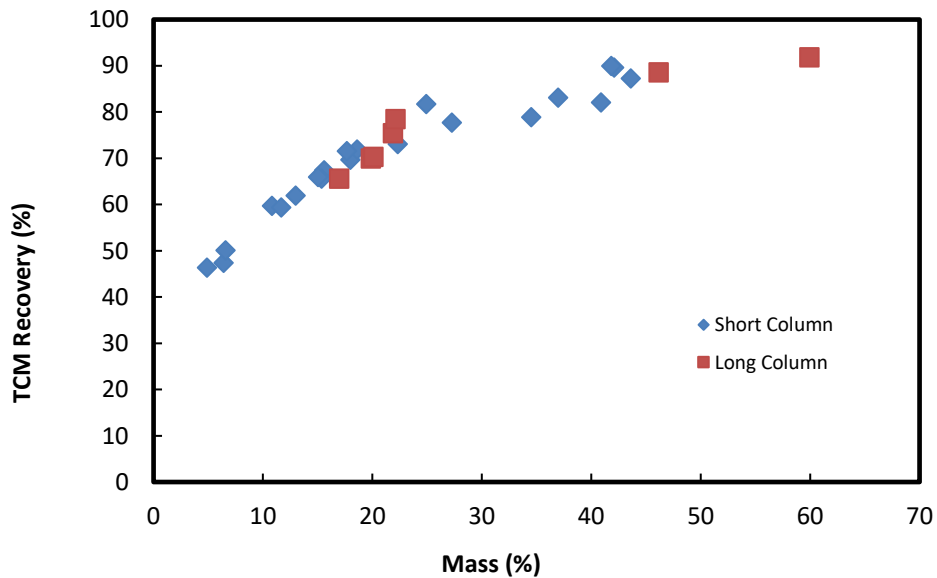


Figure 8 TCM recovery vs mass pull for short and long column

#### 4.2.5 Comparison of the Commercial bubble generator, Dual bubble generator and Denver Cell.

In this experiment, the effects of Commercial bubble generator and Dual bubble generator on flotation column and the flotation effect comparison of Denver Cell were tested. Significant data was collected from the short column with the U of A. Significant data was collected from the short column with the U of A sparger, which allows for a

comparison between Commercial bubble generator, Dual bubble generator and laboratory Denver cell.

Table 4-1 Flotation results from Commercial bubble generator, dual bubble generator and Denver cell

	Mass	Au		TCM (Corg)		S total	
	(%)	(g/t)	% Rec.	(%)	% Rec.	(%)	% Rec.
<b>Commercial bubble generator</b>							
Ro+Scav Conc.	42.96	6.14	77.17	3.72	88.33	2.23	90.56
Scav Tail	57.04	1.38	22.83	0.48	11.67	0.20	9.44
<b>Dual bubble generator</b>							
Ro+Scav Conc.	42.08	7.35	83.35	4.36	89.65	1.96	88.94
Scav Tail	57.92	1.20	16.65	0.39	10.35	0.23	11.06
<b>Denver cell</b>							
Conc.	32.23	8.34	67.26	3.85	70.39	1.81	68.23
Tails	67.77	1.93	32.74	0.77	29.61	0.40	31.77

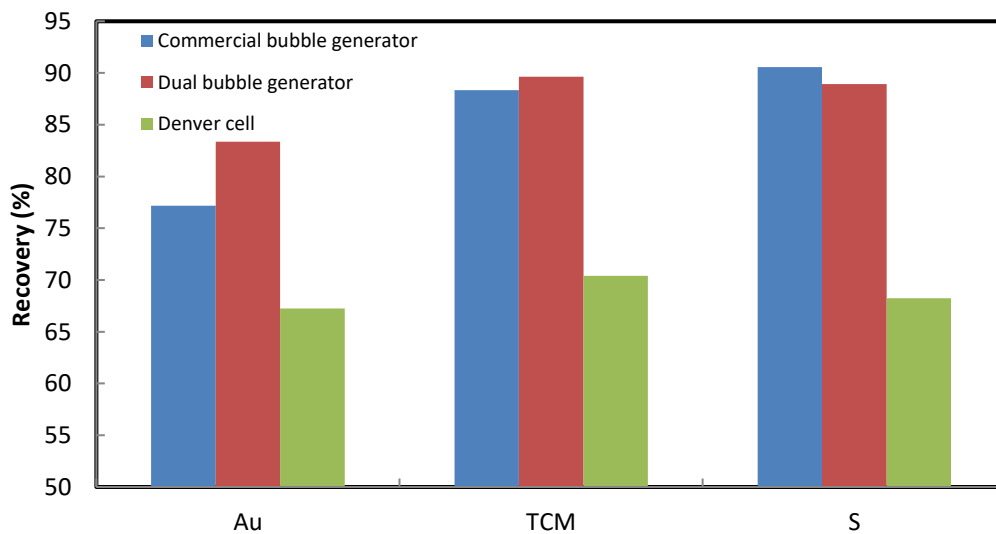


Figure 9 Au, TCM, S Recovery from flotation column with commercial bubble generator, dual bubble generator and Denver cell rougher and scavenger flotation

As shown in Figure 4-2-8, flotation column has more effect on fine particle mineral than Denver Cell. Two kinds of flotation columns with commercial bubble generator and dual bubble generator were compared. Dual bubble generator has a better flotation effect for gold and TCM The column with dual bubble generator clearly yielded a

consistently 6% higher recovery in gold, TCM compared to the column with commercial bubble generator operating with the same reagent scheme and mass pull. Since commercial bubble generator can only produce a kind of size bubble, so the effect of bubble aging can't be avoided in the process of flotation. When the bubbles are generated from the bubble generator, it is possible that the size of the mineral particle is too small to be adhered together with the particle in time. And the longer retention time of the bubble in the pulp is, the more difficult it is to contact and adhere with the mineral particles. When dual bubble generator is adopted, a number of small bubbles can be generated on the surface of a particle through a bubble generator. Increase the contact between fine particles, to increase the size of fine particles. It also quickly contacted with the flotation bubbles to avoid the negative effects of bubble aging on the combination of bubbles and mineral particles.

For comparison, the flotation tests were first conducted using a commercial hydrodynamic cavitation based sparger and a Denver flotation cell under the identical flotation reagent schemes. Gold recovery at different mass pulls by column flotation using the dual bubble generator and Denver cell flotation is shown in Figure 4-2-9. It is evident that increasing the mass pull increases gold recovery for both column flotation by dual bubble generator and Denver flotation cell, as anticipated. However, the gold recovery by column flotation is consistently higher recovery in gold than Denver cell flotation, showing superperformance.

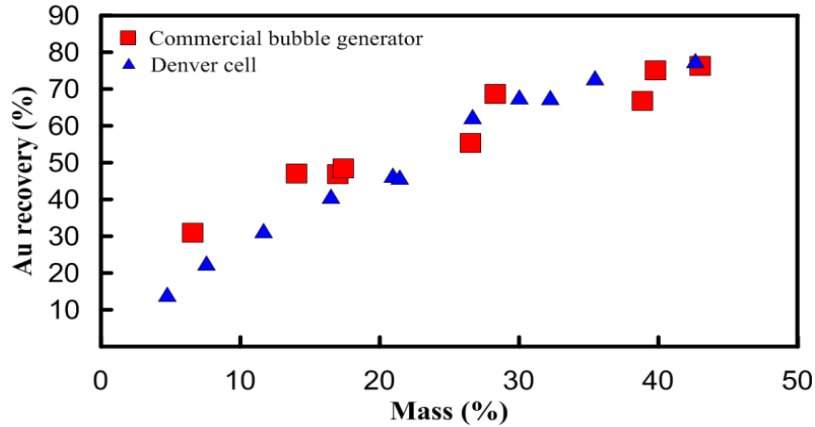


Figure 10 Effect of mass pull on gold recovery using Denver flotation cell and flotation column with commercial bubble generator

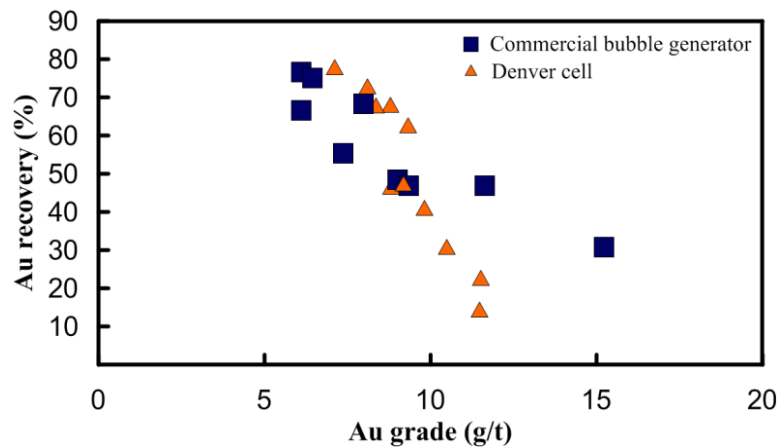


Figure 11 Gold grade-recovery curve obtained using Denver flotation cell and flotation column with commercial bubble generator

The gold grade-recovery curves obtained using Denver flotation cell and flotation column with commercial sparger are shown in Figure 4-2-10. For both Denver flotation cell and flotation column, gold grade decreases with increasing gold recovery as anticipated in the well-known grade-recovery trade-off. However, the grade-recovery curve of flotation column shifted in upright direction, indicating a better separation performance of flotation column. More micro size bubbles generated in flotation column by commercial sparger clearly is beneficial for recovering fine refractory gold. In the venturi tube based sparger, the gas nuclei was created selectively on hydrophobic

particle surfaces when slurry went through at a high flow velocity. The aggregation of hydrophobic fine particles increases the apparent sizes of fine particle aggregates with the gas nuclei acting as a bridge among the particles (Sobhy and Tao, 2013; Li et al., 2015). As a result, both recovery and selectivity of froth flotation were improved. This is the reason why the flotation column with commercial hydrodynamic cavitation sparger showed better performance than Denver cell.

One of the major limitations of venturi based cavitation tube for bubble generation is limited gas holdup to achieve high recovery. Also small bubbles suffer low rising velocity or limiting the size of particles that it can lift. It is therefore highly desirable to introduce conventional size bubbles that could be attached to gas nuclei frostered fine particle aggregates, as illustrated in our dual bubble generator shown in Figure 2-6. The flotation tests were conducted under the identical flotation chemistry using our dual bubble generator in place of commercial hydrodynamic cavitation sparger. Flotation results are shown in Figures 4-2-11 and Figure 4-2-12.

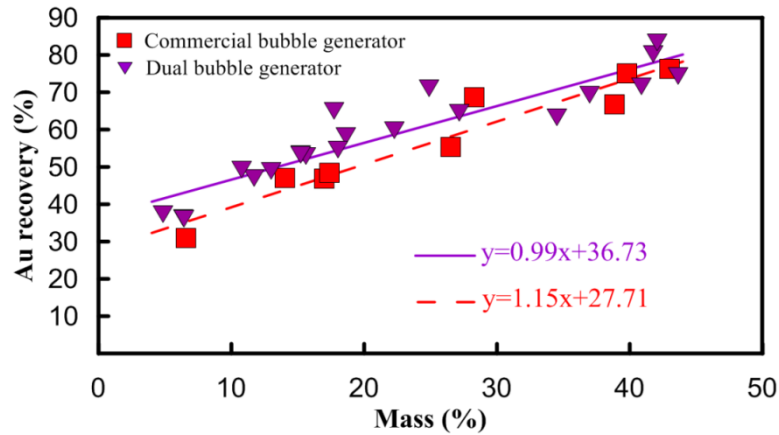


Figure 4-2-11 Effect of mass pull on gold recovery in flotation column with dual bubble generator or commercial bubble generator

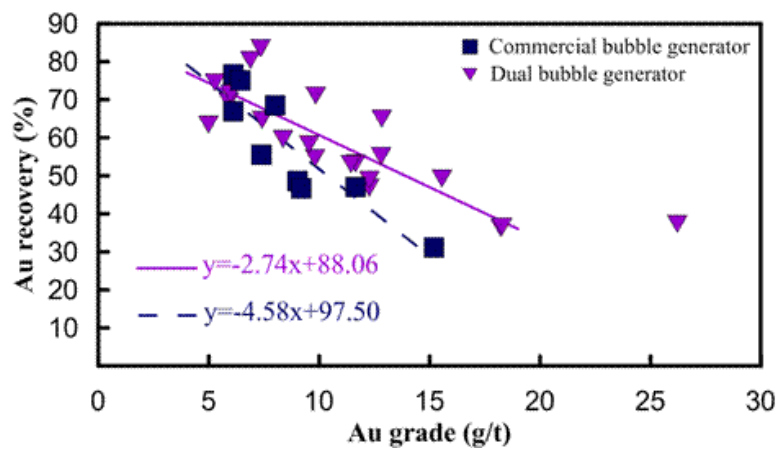


Figure 12 Gold grade-recovery curve obtained using flotation column with dual bubble generator or commercial bubble generator

Figure 4-2-11 shows a higher recovery of gold by dual bubble generator than by the commercial bubble generator at a given mass pull, more evident over low mass pull regime. To better compare the results, we fitted the data to a linear function as shown by the straight lines. The best fitted trend line of flotation column with the dual bubble generator lies above the line for commercial bubble generator, clearly showing a better recovery at a given mass pull. The superior performance obtained using the dual bubble generator confirms the advantage of added conventional flotation size bubbles to the hydrodynamic cavitation bubble generators in recovering ultrafine particles from double refractory gold ores. It appears that micro size bubbles generated on the particle

surface attached to the conventional flotation size bubbles generated in the sintered tube, as indicated in the results of Figure 4-2-10

In addition to the improvement in gold recovery at a given mass pull by flotation column with dual bubble generator, the results in Figure 4-2-12 show a significant increase in gold grade for a given gold recovery. For example at gold recovery of 60 %, a grade improvement of the concentrate from 8.35 g/t to 12.85 g/t was obtained. In general, the grade-recovery data obtained by dual bubble generator shifted to upright direction, indicating a better separation efficiency. To have a better comparison, we also fitted the data to a linear function as shown by the lines in the figure. Based on the grade-recovery trend line equations given in Figure 4-2-12, flotation column with the commercial bubble generator features a higher slope than flotation column with dual bubble generator, indicating a sharp drop in gold recovery with grade for column of commercial bubble generator. It appears that flotation of fine particles frostered with micro size bubbles by conventional flotation size bubble enhanced drainage of entrainment of fine gauge particles due to reduced bubble surface areas in the froth. The result shown in the Figures 4-2-11 and Figure 4-2-12 collectively support our design concept of using dual bubble generator to enhance fine particle flotation, exhibiting better flotation performance than aeration mechanism of single stage bubble-particle attachment.

## Chapter 5 Conclusions

In this study, the effect of the gas injection rate, gas injection point and addition of frother on the size of bubbles and minerals recovery were determined. Increasing gas injection rate and frother concentration enhanced gas holdup in the column. The size of bubble generated from hydrodynamic cavitation sparger decreases with increasing the frother concentration. Micron size bubbles and flotation size bubbles are generated from G1 port and G2 port at the same time.

The effect of different flotation methods on fine particle flotation was examined. A novel dual bubble generator was developed to enhance the gold recovery from Nevada double refractory gold ores. The dual bubble generator features immediated contact of fresh micro size bubbles generated by hydrodynamic cavitation with conventional flotation size bubbles by ceramic sparger, reducing bubble aging and hence the bubble-particle induction time. Compared with a commercial hydrodynamic cavitation based bubble generator, the dual bubble generator showed better performance, increasing both gold recovery and grade, demonstrating the potential of dual bubble generator for fine particle flotation.

## Chapter 6 Future work

Many effort have been made on revealing the performacnce of dual bubble generator during fine particle flotation. In this study, the fine particle recovery improved by using a dual bubble generator. To improve the flotation efficiency, both the gas injection point and the geometryof the hydrodynamic bubble generator are important. The ratio of inlet diameter to the throat diameter of a hyrodynamic bubble generator as well as the angle of inlet need to be investigated in the future research. In order to investigate the best location between the big bubble and small bubble generated from the sparger, the location of the gas injection ports need to be considered in the future research.

Through this study, gold recovery improved by using dual bubble generator. Studies on reagent optimization or developing new reagents to improve hydrophobic properties are recommended. Considering the mineral particle size, the different sizes of mineral particle should be tested by using dualbubble generator in the next step.

## References

- Bailey, M., Gomez, C. and Finch, J. (2005). A method of bubble diameter assignment. *Minerals Engineering*, 18(1), pp.119-123.
- Brennen, C. (2014). *Cavitation and bubble dynamics*. New York: Cambridge University Press.
- Coffin, V.L., (1982). Column flotation at Mines Gaspe. In: XIV International mineral processing congress. Toronto, Canada. Paper 4-21
- ERIEZ 2013, CPT Cavitation System. <<http://efd.eriez.com/products/index/cavitationtube>>.
- Eriezflotation.com (2015). *CavTube Sparging | Eriez Flotation Division*. Retrieved 31 December 2015, from <http://www.eriezflotation.com/sparging/cavtube-sparging>
- Feng, D. and Aldrich, C. (1999). Effect of particle size on flotation performance of complex sulphide ores. *Minerals Engineering*, 12(7), pp.721-731.
- Finch, J. (1995). Column flotation: A selected review— part IV: Novel flotation devices. *Minerals Engineering*, 8(6), pp.587-602.
- Gogate, P. and Pandit, A. (2001). HYDRODYNAMIC CAVITATION REACTORS: A STATE OF THE ART REVIEW. *Reviews in Chemical Engineering*, 17(1), pp.1-85.

- Gogate, P. and Pandit, A. (2004). Sonophotocatalytic reactors for wastewater treatment: A critical review. *AIChE Journal*, 50(5), pp.1051-1079.
- Hu, H., Finch, J., Zhou, Z. and Xu, Z. (1998). Numerical and experimental study of a hydrodynamic cavitation tube. *Metallurgical and Materials Transactions B*, 29(4), pp.911-917.
- Kress, T.S., 1972. Mass Transfer between Small Bubbles and Liquids in Cocurrent Turbulent Pipe Flow. University of Tennessee, Tennessee.
- Li, H., Afacan, A., Liu, Q. and Xu, Z. (2015). Study interactions between fine particles and micron size bubbles generated by hydrodynamic cavitation. *Minerals Engineering*, 84, pp.106-115.
- Li, Jingjing, (2017). Investigation on the effect of geometrical parameters on the performance of a venturi type bubble generator, *Nuclear Engineering and Design* 325 (2017) 90–96.
- Luttrell, G., & Yoon, R. (1992). A hydrodynamic model for bubble—particle attachment. *Journal of Colloid and Interface Science*, 154(1), 129-137.
- Manlapig, E.V., Spottiswood, D.J., (1978). *Present practices in the computer control of copper flotation plants*. SME-AIME fall meet, Lake Buena Vista.
- Melo, F. and Laskowski, J. (2006). Fundamental properties of flotation frothers and their effect on flotation. *Minerals Engineering*, 19(6-8), pp.766-773.

- Moholkar, V. and Pandit, A. (1997). Bubble behavior in hydrodynamic cavitation: Effect of turbulence. *AIChE Journal*, 43(6), pp.1641-1648.
- Nesset, J., Hernandez-Aguilar, J., Acuna, C., Gomez, C. and Finch, J. (2006). Some gas dispersion characteristics of mechanical flotation machines. *Minerals Engineering*, 19(6-8), pp.807-815.
- Niemi, A. and Paakinen, U. (1969). Simulation and control of flotation circuits. *Automatica*, 5(5), pp.551-561.
- Polli, M., Stanislao, M., Bagatin, R., Bakr, E. and Masi, M. (2002). Bubble size distribution in the sparger region of bubble columns. *Chemical Engineering Science*, 57(1), pp.197-205.
- Sobhy, A. and Tao, D. (2013). High-Efficiency Nanobubble Coal Flotation. *International Journal of Coal Preparation and Utilization*, 33(5), pp.242-256.
- Tao, D. (2004). Role of Bubble Size in Flotation of Coarse and Fine Particles—A Review. *Separation Science and Technology*, 39(4), pp.741-760.
- Tao, Y., Liu, J., Yu, S. and Tao, D. (2006). Picobubble Enhanced Fine Coal Flotation. *Separation Science and Technology*, 41(16), pp.3597-3607.
- Tao, D., Yu, S., Zhou, X., Honaker, R., & Parekh, B. (2008). Picobubble Column Flotation of Fine Coal. *International Journal of Coal Preparation and Utilization*, 28(1), 1-14.

- Tavera, F., Escudero, R. and Finch, J. (2001). Gas holdup in flotation columns: laboratory measurements. *International Journal of Mineral Processing*, 61(1), pp.23-40.
- Unno, H. and Inoue, I. (1980). Size reduction of bubbles by orifice mixer. *Chemical Engineering Science*, 35(7), pp.1571-1579.
- Wang, L. (2013). *A study of interactions between an air bubble and a solid surface in a liquid*. University of Alberta, Edmonton, Dissertation for **Doctor of Philosophy**.
- Wang, A., Yan, X., Wang, L., Cao, Y., Liu, J., (2015). Effect of cone angles on single-phase flow of a laboratory cyclonic-static micro-bubble flotation column: piv measurement and CFD simulations. *Sep. Purif. Technol.* 149, 308–314.
- Weber, M. and Paddock, D. (1983). Interceptional and gravitational collision efficiencies for single collectors at intermediate Reynolds numbers. *Journal of Colloid and Interface Science*, 94(2), pp.328-335.
- Xu, Z., Choung, J., Sun, W., Cui, Z., (2006a). Role of hydrodynamic cavitation by high intensity agitation in fine particle aggregation and flotation. In: XXVII International Mineral Processing Congress, Istanbul, Turkey.
- Yan, X., Liu, J., Zhou, C., (2012) . Two-phase numerical simulation on the pipe flow unit of cyclonic static micro bubble flotation column. *J. Chin. Coal Soc.* 37, 506–510,

- Yianatos, J., Bergh, L., Condori, P. and Aguilera, J. (2001). Hydrodynamic and metallurgical characterization of industrial flotation banks for control purposes. *Minerals Engineering*, 14(9), pp.1033-1046.
- Yoon, R. and Luttrell, G. (1986). The Effect of Bubble Size on Fine Coal Flotation. *Coal Preparation*, 2(3), pp.179-192.
- Yoon, R., Flinn, D. and Rabinovich, Y. (1997). Hydrophobic Interactions between Dissimilar Surfaces. *Journal of Colloid and Interface Science*, 185(2), pp.363-370.
- Zhou, Z., Egiebor, N. and Plitt, L. (1993). Frother effects on bubble size estimation in a flotation column. *Minerals Engineering*, 6(1), pp.55-67.
- Zhou, Z., Xu, Z., Finch, J., Hu, H., & Rao, S. (1997). Role of hydrodynamic cavitation in fine particle flotation. *International Journal of Mineral Processing*, 51(1-4), 139-149.
- Zhou, Z.A., Chow, R.S., Su, N., (2005). Spontaneous bubble nucleation on bitumen surfaces, *Report for CONRAD Extraction Technology Group*, Alberta Research Council.
- Zhou, Z.A., Chow, R.S., (2006b). Effect of shear on bitumen–bubble attachment in model systems. *Final Report for CONRAD Bitumen Production Technical Group*, Alberta Research Council.

Zhou, Z., Xu, Z., Finch, J., Masliyah, J. and Chow, R. (2009). On the role of cavitation in particle collection in flotation – A critical review. II. *Minerals Engineering*, 22(5), pp.419-433.

Zhou, Z., Chow, R., Cleyle, P., Xu, Z., & Masliyah, J. (2010). Effect of Dynamic Bubble Nucleation on Bitumen Flotation. *Canadian Metallurgical Quarterly*, 49(4), 363-372.

## Appendix

### MATLAB code.

A MATLAB program was developed to calculate the bubble size based on the image we take from the high speed camera in the McGill bubble size analyzer.

```
clear
close all
addpath('./Pics');

%% basic parameters
picName = '1.jpg'; % picture name
maxCircleD = 60; % max bubble size(pixel)
minCircleD = 10; % min bubble size(pixel)
scale_pix = 1; % set 1mm=10pxial
theta = 0.5; %
%% read pic
im = imread('1.jpg');
bw = im2double(rgb2gray(im));

%% frangi
options = struct('FrangiScaleRange', [0.5 5], ... %
                'FrangiScaleRatio', 1, ... %
                'FrangiBetaOne', 0.4, ... %beta 1
                'FrangiBetaTwo', 0.01, ... %beta 2
                'verbose',true,'BlackWhite',true);

J=FrangiFilter2D(bw,options);

J = imadjust(J,stretchlim(J],[0 1]);
imshow(J)
title('frangi')

%% Circle
a = minCircleD:maxCircleD;
cPatches = cell(1,length(a));
N_cPatches = zeros(1,length(a));
for i = 1:length(a)
    if i<20
        [cPatches{i},N_cPatches(i)] = circlePatch(a(i),1);
```

```

else
    [cPatches{i},N_cPatches(i)] = circlePatch(a(i),2);
end
end

%%
outimg = cell(1,length(a));
allImg = zeros(size(J));
for i = 1:length(a)
    outimg{i} = conv2(J,cPatches{i},'same')/N_cPatches(i)>theta;
    allImg = allImg + outimg{i};
end

allImg = allImg>0;

%
bw2 = bw;
bw2(allImg) = 1;
figure
imshow(bw2);
title('centre')

% Find centroid
L = bwlabel(allImg);
S = regionprops(L,'Centroid');
centroids = cat(1, S.Centroid);
figure
imshow(im);
hold on
plot(centroids(:,1), centroids(:,2), 'b*')
hold off

% distribution
Rs = zeros(1,size(centroids,1));
for i = 1:size(centroids,1)
    x = round(centroids(i,2));
    y = round(centroids(i,1));
    r = [];
    for j = 1:length(outimg)
        if sum(sum(outimg{j}(x-1:x+1,y-1:y+1))) >0
            r = [r,size(cPatches{j},1)/2];
        end
    end
end

```

```

    end
    Rs(i) = mean(r);
end
Rs = Rs/scale_pix;

figure
hist(Rs,20);
title('bubble size distribution');
xlabel('bubble diameter [mm]');
ylabel('counts');

figure
imshow(im);
hold on
plot(centroids(:,1), centroids(:,2), 'b+')
for i = 1:size(centroids,1)
    text(centroids(i,1),centroids(i,2),num2str(Rs(i)));
end
hold off

```